# Multiply structural optimized strategies for bismuth oxyhalide photocatalysis and their environmental application

Ziwei Wang [a,b,1], Ming Chen [a,b,1], Danlian Huang [a,b,1], Guangming Zeng [a,b*], Piao Xu [a,b*] , Chengyun Zhou [a,b], Cui Lai [a,b], Han Wang [a,b], Min Cheng [a,b], Wenjun Wang [a,b]

[a] *College of Environmental Science and Engineering, Hunan University, Lushan South Road, Yuelu District, Changsha 410082, P. R. China*

[b] *Key Laboratory of Environmental Biology and Pollution Control (Hunan University), Ministry of Education, Lushan South Road, Yuelu District, Changsha 410082, P.R. China*

* Corresponding author.

Tel.: +86 731 88822754; fax: +86 731 88823701.

E-mail addresses: zgming@hnu.edu.cn (G. Zeng) and piaoxu@hnu.edu.cn (P. Xu).

[1]These authors contribute equally to this article.

**Abstract:**

Bismuth oxyhalide (BiOX) photocatalysts have attracted tremendous attentions due to their unique optical and electronic properties. However, pristine BiOX suffered from inherent drawbacks and unsatisfactory photocatalytic performance. Interest in engineering layered structure BiOX for efficient environment remediation has grown exponentially. Recent studies tend to focus on alloying, bismuth-rich strategies, defect introduction, element doping. Therefore, the aim of this review is to summarize multiply structural optimized strategies for the improvement of their photocatalytic applications in environmental remediation. The distinct photochemical properties and synthesis method of alloyed, bismuth-rich, doped and defect-introduced BiOX are detailly elaborated based on the discussion of the structure-property relationship. The other methods such as heterojunction, facet effect, surface plasmonic resonance and strain engineering are briefly introduced. Subsequently, environmental applications in aquatic pollutants photodegradation and air purification are also discussed. Finally, challenges and outlooks covering synthetic strategies, characterization, and applications are featured.

**Keywords:** Structural optimized strategies; Bismuth oxyhalide; Environmental remediation; Photocatalysis.

## Contents

1 Introduction

2 Multiple structural optimized strategies for the enhancement of photocatalytic activity

  2.1 Alloyed BiOX

  2.2 Bismuth-rich BiOX ($Bi_xO_yX_z$)

  2.3 BiOX with defect introduction

  2.4 BiOX with element doping

  2.5 Other methods

    2.5.1 Heterojunction

    2.5.2 Facet effects

    2.5.3 Surface plasmonic resonance

    2.5.4 Strain engineering

3 Environmental application of BiOX

  4.1 Photodegradation of aquatic pollutants

  4.2 Photocatalytic air purification

5 Summary and outlook

Acknowledgements

References

## 1 Introduction

With growing concerns regarding environmental pollution, technologies with high efficiency and sustainable development to reduce the pollutant contents of wastewater are urgently needed [1, 2]. Among the various decomposition techniques to clean-up wastewater and polluted air, semiconductor photocatalysis has received worldwide attention on the direct utilization of solar energy [3, 4]. In semiconductor photocatalysis, the toxic organic compounds can be efficiently converted into less toxic molecules or even totally completely mineralized under suitable conditions [5, 6]. Undoubtedly, the key parameter for excellent visible light induced photocatalysis is the reasonable design of efficient photocatalysts [7]. Bismuth-based materials with excellent capacity of visible light absorption and separation of charge carriers may present ideal performance to address the environment issue. Compared to conventional photocatalysts ($TiO_2$ and ZnO), they are more applicable in water splitting [8], $CO_2$ reduction [9], nitrogen fixation [10], harmful pollutant decomposition [11-13], and organic synthesis [14]. The most reported bismuth-based photocatalysts include $Bi_2S_3$, $Bi_2O_3$, $Bi_2MO_6$ (M=Cr, Mo, W), $BiPO_4$, $BiVO_4$, $Bi_xTiO_y$, $(BiO)_2CO_3$, BiOX (X = Cl, Br, I), etc. Our team also synthesized g-$C_3N_4$/$Bi_2WO_6$ [15], $WO_3$/g-$C_3$N4/$Bi_2O_3$ [16], and Bi/BiOCl/$ZnSn(OH)_6$ [17] for the photodegradation of refractory pollutants.

Bismuth oxyhalide, as a remarkably multi-component V–VI–VII semiconductors, have been extensively studied due to typical layered structure and superior carrier transport properties [18]. They have excellent chemical stability, nontoxicity, and resistance to corrosion. The structures of BiOX are crystallized in a tetragonal matlockite (PbFCl-type) consisting of [Bi-O] layers interleaved with two halogen atom slabs [19]. It's worth noting that the strong intralayer covalent bonding and the weak interlayer van der. Waals interaction exist in the layered structure. Therefore, this open-layer crystalline structure is available for facilitating the reasonable structural design of both [Bi-O] and halogen layers [20, 21]. Compared to other bismuth-based materials, BiOX possess a tunable band gaps of BiOCl, BiOBr, and BiOI (around 3.3 eV, 2.6 eV, and 1.8 eV, respectively), implying that they are promising visible-light-driven photocatalysts [22].

The pioneering application of BiOCl in environment remediation is firstly reported by Huang et al. [19] in 2006, although the history of photocatalysis can be traced back to 1972 [23]. Subsequently, Zhang’s group systematically investigate the photocatalytic activity of BiOX-based materials with hierarchical microspheres superstructures for the efficient degradation of methyl orange (MO) [24]. Since then, intense researches have been developed on the BiOX-based photocatalysis. Nowadays, a series of morphology-controlled BiOX, such as 1D templated nano-fibers/wires [25], 2D intrinsic nanostructures [26, 27], 3D assembled hierarchical architectures [28, 29] and supported thin films [30, 31] have been synthesized to maximize the photocatalytic application. The multiple morphologies generally provide the large specific surface area and rich reactive sites [32]. At the same time, numerous semiconductors have been coupled with BiOX to further promote the separation of electron-hole pairs across the solid-solid heterogeneous interface structure [33-36]. Unfortunately, some BiOX suffered from poor light absorption and rapid recombination possibility for the electron-holes, which tremendously limited their industrial application [37-40]. Thus, more and more studies are focused on layered structure design of BiOX to overcome these obstacles so as to provide insight on the relationship between structural characteristics and the photocatalytic properties.

The first critical issues related to the photocatalytic activity of BiOX are the evolution of band gaps. The band structures such as valence band (VB), conduction band (CB) and band gap commonly determine the inherent photoexcitation, migration of carriers and the redox capacities of electron-hole pairs [41, 42]. Regarding optical absorption, the response wavelengths of BiOCl exist in the UV light region due to the wide band gap. Although BiOBr and BiOI have a narrowed band gap, the inherent rapid recombination possibility for the electron-holes and the incompatible band-edge positions for targeted redox reaction still hinder their application. To address these challenges, solid solutions, bismuth-rich strategies and doping with various elements are available approaches for precise adjustment of the bandgap and the band-edge band positions. Furthermore, the introduced defects could act as a shallow donor that offer the local excited charges to enhance visible light absorption.

Another key issues relevant to the photocatalytic capacity of BiOX is the surface/interface engineering. The exposed facets on BiOX play crucial roles in the charge carriers separation and transportation, governing the selectivity and rate of photocatalysis reaction [43]. The photoactivity contrast investigation of BiOCl nanosheets with dominant (001) and (010) facets by pH modulation has been recognized as the land mark event [22]. Since then, many attempts to reasonably fabricate BiOX with specific exposed facets such as 001 faceted BiOCl [44], 102 faceted BiOBr [45] and 110 faceted BiOI [46] have been developed with a capping agent of $H^+$. More interesting, Zhang's group also investigated the facet effects of BiOCl in detail and reported a correlation relationship between the facet exposure and internal electric field (IEF). Following, bismuth-rich strategies and doping with various elements also provide a perfect platform for tuning IEF to enhance bulk-charge separation (BCS) efficiency. In general, the stronger internal electric field yields the faster photocatalytic process. Furthermore, surface defect introduction is another efficient modulation strategy. It could act as direct coordinating sites for enhanced adsorption of typical molecules like $N_2$, $O_2$, $CO_2$ and $H_2O$.

In recent years, reviews about BiOX photocatalytic materials with diverse topics in modification [47], facet effects [48], energy and environment application [43, 49], nanostructure [50], layered structure [51-54] and bismuth-rich strategies [55] have been published before. As illustrated in Fig. 1, interest in methods of BiOX with energy band and surface/interface engineering (alloying, bismuth-rich strategies, doping and defect-introduction) in photocatalysis has grown exponentially. However, these methods and the related environmental application of this series of photocatalysts have scarce been systematically reviewed. In this review, we explore how these strategies are exploited to improve the photocatalytic performance of BiOX based on the structure-property correlativity discussion. The adjustive principle and key parameters for structural design are also highlighted. Then, recent advances in environmental application of BiOX-based photocatalysts are elaborated. Finally, challenges and outlooks covering synthetic strategies, characterization, and applications are featured.

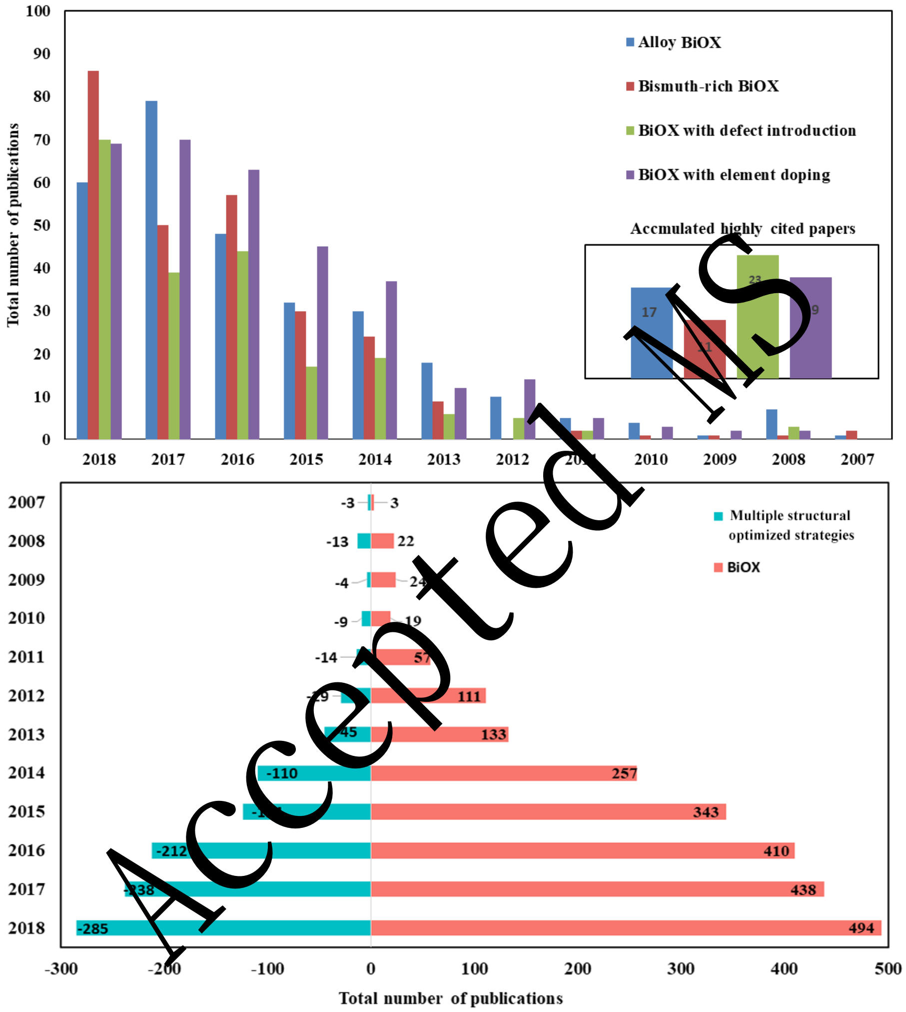

Fig. 1. Increasing interest in engineering in the layered structure of BiOX. The chart displays the total number of publications year about alloyed, bismuth-rich, doped and defect-introduced BiOX (a) and the total number of publications per year about multiple structural optimized strategies of BiOX comparing to pristine BiOX.

## 2 Multiple structural optimized strategies

Fig. 2 illustrated the different schematic diagram of BiOX with various engineering layered structure [56]. As shown in Fig. 2a, BiOX are consisted of [$Bi_2O_2$] layers interleaved with two halogen atom slabs. For alloyed $BiOCl_xBr_{1-x}$, Cl atoms in the supercell are partially substituted with Br atoms (Fig. 2b). Fig. 2c displays unique layered structure of non-metal ion doped $Bi_3O_4Cl$. In this crystal structure, enriched [Bi-O] layers are placed between double slabs of chlorine ions and foreign ions. Compared to traditional BiOCl, the existence of oxygen vacancies (OVs) significantly shorten the lengths of Bi-O and Bi-Bi, thus altering their chemical and optical properties (Fig. 2d). These changes in crystal structure efficiently optimize energy band configuration and surface structure, which endow BiOX with excellent separation and migration of electron-hole pairs and suitable band-edge position for targeted photocatalytic reaction.

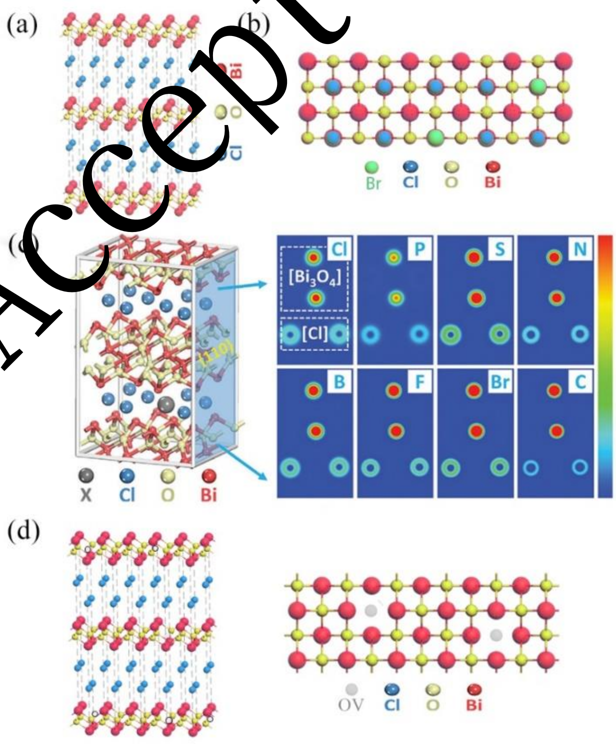

Fig. 2. Different structure of BiOCl. Schematic illustration of the (a) Primitive cell of BiOCl and

(b) Schematic representation of top view of the crystal structure of $BiOCl_xBr_{1-x}$ (c) $Bi_3O_4Cl$ crystal structure and charge density contour plots [56] (d) Schematic representation of top and side view of the structure of BiOCl with surface oxygen vacancies. Reprinted with permission from Wiley-VCH.

## 2.1 Alloyed BiOX

For the past decades, alloyed semiconductor nanomaterials have made enormous progress as a typical bandgap engineering with tunable compounds [57]. For alloyed BiOX, halogen atoms in the supercell are partially substituted with another exogenous halogen atoms. Benefitting from electronic structure and atomic arrangement, it is easy for halogen atoms to replace each other into BiOX layered structure, leading to nearly discretionary variation of halogen ions [58]. Currently, various alloyed BiOX, including $BiOCl_xBr_{1-x}$, $BiOI_xCl_{1-x}$, $BiOBr_xI_{1-x}$ and $BiO(ClBr)_{(1-x)/2}I_x$ have been synthesized and found to show higher activity than the corresponding pure forms. Zhang et al. [59] suggested that higher photocatalytic activity of alloyed BiOX depended on the regulation of band gaps. Based on the density functional theory (DFT) computations, the band gaps decreased with an increasing content of heavier halogen atoms (Fig. 3), which led to significant red-shift of adsorption spectra and higher sunlight utilization efficiency. Besides, the constitution of VB for BiOX contained primary O 2p and X np orbitals [37], which made the VB tops more positive with the increase of the lighter halogens, indicating a stronger oxidation ability [59, 60].

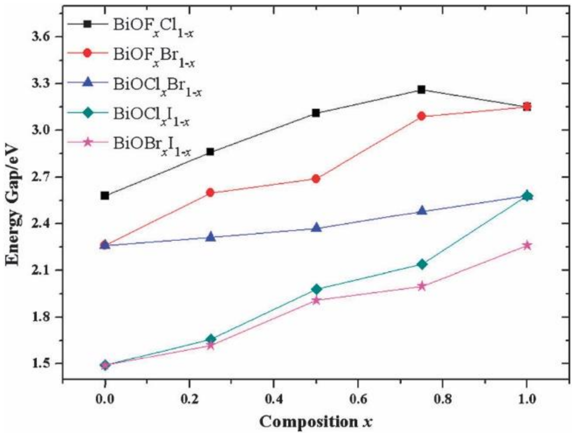

Fig. 3. The variation of the band gaps with the composition, x, for alloyed BiOXs. x = 0 and 1 represents the pure BiOX crystals [59]. Reprinted with permission from the Royal Society of Chemistry.

Another important common feature of alloyed BiOX is their excellent separation of electron–hole pairs [61]. It may be ascribed to the hybridization of the X np states which leads to a smaller valence band maximum (VBM) and stronger chemical disorder in alloyed BiOX. The disorder and variation in VBM may cause the defect levels which act as trap centers for photogenerated holes thus hindering the mobility of the photoexcited holes within the alloyed BiOX to reduce the electron–hole recombination. For instance, Wang et al. [62] showed that OV-rich BiOBr$_{0.85}$I$_{0.15}$ possessed the highest photocurrent density and the smallest radius in the electrochemical impedance spectra compared to BiOBr, BiOI and OV-poor BiOBr$_{0.85}$I$_{0.15}$, which meant a longer lifetime of photoinduced charge carriers at BiOBr$_{0.85}$I$_{0.15}$.On the one hand, the alloying effect in BiOX brings about a substantially lower electron-hole recombination rate and thus a much higher photocatalytic activity. On the other hand, alloyed BiOX are easier to format OVs, which act as a capture trap for photo-generated electrons to promote the separation of charge carriers.

In 2011, Shenawi-Khalil and co-workers [63], for the first time, introduced a new family of $BiO(Cl_xBr_{1-x})$ nanomaterials via hydrothermal route. After that, we have witnessed the rising interest in $BiOX_xY_{1-x}$ (X, Y = Cl, Br, and I) with superior optical absorption property and optical stability. The usual synthesis methods for alloy BiOX, such as precipitation, hydrothermal and solvothermal routes, are listed in Table 1. The point of facilely achieving high-quality alloyed compounds is the similarities of the lattice constant between the substrate material and the material to be grown. Hence, halogen sources including KX, NaX, $NH_4X$, CTAX (X = Cl, or Br) or ionic liquids ($C_{16}$[Mim]Cl and $C_{16}$[Mim]Br) are widely used for the synthesis of alloy BiOX. And the obtained alloyed BiOX photocatalysts display diversified morphologies and excellent band energy. To confirm the main influence factors and develop environmental-friendly facile synthesis, the guide and perfection of synthesis factors is very important. Referred to Table 1, two key experimental variables are suggested, viz. (I) the proportion and kinds of reagents offering halogen atoms (II) the control of reaction conditions including, temperature, time, solvent used for preparation and the pH of the reaction solution.

To clarify the relationship between different experimental variables and the properties of alloyed BiOX, a series of studies have been reported. For example, $BiOCl_{0.875}Br_{0.125}$ [64] was synthesized by a quite simple stirring at room temperature. The committed step was completely dissolving $Bi(NO_3)_3•5H_2O$ to form intermediate species $[Bi_2O_2]^{2+}$, via using glacial acetic to facilitate an instant reaction of $Bi^{3+}$, water and the halide anions. Moreover, as common structure-directing agents, CTAC and CTAB are also supplied as the halides source. Recently, Yang [65] prepared various $BiOCl_xBr_{1-x}$ to reveal the effects of raw materials and solvents. They found out that $NH_4Cl$, KBr and water tended to guide simple stacking with nanoplates, while polyacrylamide (C-PAM), CTAB and glycol were inclined to form 3D hierarchical flower-like microspheres. In principle, hierarchical flower-like structure endows BiOX with larger specific surface area and more active sites, thus boosting photocatalytic reactions. Liu et. al firstly synthesized alloyed $Bi_{24}O_{31}Cl_xBr_{10-x}$ [66] by dissolving appropriate amounts of $Bi(NO_3)\cdot 5H_2O$, CTAB and CTAC into ethylene glycol at 160°C for 16 h. These works evidently demonstrated that alloyed BiOX photocatalytic activity is mainly contingent on the fabrication protocol and nature of the source materials.

## 2.2 Bismuth-rich BiOX

As well known, band structure is pivotal for the energy utilization efficiency and photocatalytic properties of semiconductor. Based on the DFT calculations of BiOX, the upper VB is primarily composed of hybridized O 2p orbitals and X np (n = 3, 4, and 5 for X = Cl, Br, and I) orbitals; whereas the CB is based on the Bi 6p orbitals [67]. This calculation suggests that an effective way to decrease the band gap of BiOX is to adjust the relative amounts of bismuth, oxygen and chloride. Therefore, bismuth-rich strategy ($Bi_xO_yX_z$) with increasing in the content of bismuth may change the bandgap energy, endowing a more negative CB positions with stronger reducing ability of the electrons [68-70]. Recently, first-principles calculations exhibited hybridized Bi 6p and Br 4s orbitals on the $Bi_{24}O_{31}Br_{10}$ [71], thus upshifting CB to achieve the application of water splitting.

In addition, bismuth-rich strategies also provide a perfect platform for tuning IEF to enhance BCS efficiency. The hybridization of the Bi 6s and O 2p levels induces a highly dispersed VB that increases the mobility of photo-induced holes in VB and hence favors oxidation reaction in photocatalysis [72]. Furthermore, the enhancement of IEF relied on $Bi_xO_yX_z$ (X = Cl, Br, I) is also important for the improvement of photocatalytic activity. In general, the migration pathway of charge carriers includes the bulk and the surface of photocatalysts. The charge separation efficiency increases with the enhancement of IEF, especially for BCS. For $Bi_xO_yX_z$, the expanded interlamellar spacing and dipole moment endow it with strong IEF perpendicular to $[X_m]$ layers to promote excellent separation of electron-hole pairs. Therefore, studies have widely focused on bismuth-rich bismuth oxyhalide materials, and a series of novel $Bi_xO_yX_z$ photocatalysts were synthesized.

We summarized the synthesis process of bismuth-rich bismuth oxyhalide in Table 1, including hydrothermal and solvothermal process [67, 73-82], calcination process, microwave synthesis [69, 83, 84], and molecular precursor synthesis [85-90]. Within these processes, the reaction time, reaction temperature, nature of reaction solvents, solution pH and reactant mole ratio play key roles in obtaining $Bi_xO_yX_z$ (X=Cl, Br, I) [67, 73-82] (Table 1). Solution pH plays an important role in the hydrothermal process. Commonly, alkalization regulation is almost the most widely used methods in hydrothermal process using bismuth salts ($Bi(NO_3)_3{\bullet}5H_2O$ and $BiX_3$) as bismuth source. Earlier in 2003, Wang and Li [91] investigated the composition of ternary bismuth oxybromide controlled by pH adjusting using the cationic surfactant cetyltrimethylammonium bromide (CTAB) as the bromine source. As a result, $Bi_{24}O_{31}Br_{10}$ nanobelts were obtained at pH 8–10 by hydrothermal method, $Bi_3O_4Br$ were prepared at 11–12, while the pH increased to 13-14, $Bi_{12}O_{17}Br_2$ nanobelts were gained, whereas at lower pH<7 and replacing CTAB with NaBr, only BiOBr nanoplates were obtained at various pH conditions. They suggested that formation of $CTA^+OH^-$ might be suitable for the growth of bismuth oxide bromide nanobelts. Normally, $Bi^{3+}$ first reacted with $H_2O$ and halide ions to yield BiOX, with the increasing of pH, the halogen ions in BiOX are gradually replaced by $OH^-$ leading to the formation of $Bi_xO_yX_z$. A series of $Bi_4O_5X_2$, $Bi_{24}O_{31}X_{10}$, $Bi_3O_4X$, $Bi_5O_7X$, $Bi_{12}O_{17}X_2$ and finally a-$Bi_2O_3$ could be synthesized when the amount of ammonia was sufficient. The inferential pathways of the formation of $Bi_xO_yX_z$ are elucidated as follows:

$$Bi^{3+} + 3OH^- \rightarrow Bi(OH)_3 \tag{1}$$

$$2Bi(OH)_3 + X^- \rightarrow BiOX + H_2O + OH^- \tag{2}$$

$$Bi^{3+} + 3X^- \rightarrow BiX_3 \tag{3}$$

$$BiX_3 + 2OH^- \rightarrow BiOX + 2X^- + H_2O \tag{4}$$

$$4BiOX + 2OH^- \rightarrow Bi_4O_5X_2 + 2X^- + H_2O \tag{5}$$

$$6Bi_4O_5X_2 + 2OH^- \rightarrow Bi_{24}O_{31}X_{10} + 2X^- + H_2O \tag{6}$$

$$Bi_{24}O_{31}X_{10} + 2OH^- \rightarrow 8Bi_3O_4X + 2X^- + H_2O \tag{7}$$

$$5Bi_3O_4X + 2OH^- \rightarrow 3Bi_5O_7X + 2X^- + H_2O \tag{8}$$

$$12Bi_5O_7X + 2OH^- \rightarrow 5Bi_{12}O_{17}X_2 + 2X^- + H_2O \tag{9}$$

$$Bi_{12}O_{17}X_2 + 2OH^- \rightarrow 6Bi_2O_3 + 2X^- + H_2O \tag{10}$$

Actually, BiOX materials with increased Bi contents, such as $Bi_3O_4Cl$, $Bi_{12}O_{17}Cl_2$, $Bi_{12}O_{17}Br_2$, $Bi_5O_7Br$, $Bi_{24}O_{31}Br_{10}$, have been prepared at alkaline condition using bismuth salts as bismuth source. In contrast, while using α-$Bi_2O_3$ as bismuth source, acid addition might favor the synthesis of bismuth-rich BiOX using the halogen to replace the oxygen under an appropriate acidic condition. For example, Xiao’ s group [67] synthesized a serious of $Bi_xO_yX_z$ by one-pot hydrothermal route using $Bi_2O_3$ as bismuth resource via changing the amount of nitric acid. With the increase of $HNO_3$, $Bi_2O_3$ gradually was transformed to basic bismuth (III) nitrate and then BiOX, and the $Bi_xO_yX_z$ were finally synthesized with sufficient $HNO_3$ addition. For example, with the increasing $HNO_3$ addition ranging from 0.33 to 1 mmol, $Bi_5O_7I$, $Bi_7O_9I_3$ and $Bi_4O_5I_2$ and BiOI were prepared. Especially, $Bi_7O_9I_3$ and $Bi_4O_5I_2$ demonstrated superior bisphenol-A degradation ability than others due to their relatively narrower band gap energy and stronger oxidation ability.

Meanwhile, calcination treatment of BiOX and/or $Bi_2O_3$ is another widely used route to realize bismuth-rich strategies. Because of the weak van der Waals interactions between the halogen atoms, the halogen could be easily removed or replaced in BiOX. For example, Lin et al. [92] synthesized $Bi_3O_4Cl$ by calcination method which used $Bi_2O_3$ and BiOCl as raw materials to calcine at 700 ℃ in air. The prepared photocatalysts possesses an improved visible-light-driven photocatalytic activity via the regulation of band structure. The hybrid states in $Bi_3O_4Cl$ can lead to the fair dispersions in the conduction, and the valence band, consisting of Cl 3p, O 2p and Bi 6s orbitals, which might favor a fair mobility of photogenerated charges and separations of electron-hole, thus improving the photocatalytic ability.

Besides, microemulsion and molecular precursor methods could realize accurate tailored morphology and band structures. Fig. 4 illustrates the following four photocatalysts morphology formation process in detail. Mao et al. controlled the morphologies of $Bi_4O_5Br_2$ [77] via increasing the amount of surfactant TX-100 addition (Fig. 4a). The surfactant TX-100 stabilizes variable ions in microemulsions and the concentration of TX-100 control the morphologies of $Bi_4O_5Br_2$ nanomaterials. Single-crystal $Bi_3O_4Br$ nanorings [78] have been synthesized by a simple solvothermal method through a 3-steps process including formation of precursors, selective etching and Ostwald ripening. Moreover, it has been reported that BiOCl can be assembled into $Bi_{24}O_{31}Cl_{10}$ hollow microspheres via a 600°C calcination using carbonaceous materials as sacrificial templates [86]. More interestingly, with the assistant of water, 5 nm diameter $Bi_5O_7Br$ nanotubes [93] was successfully self-assembled under a low-temperature stirring condition. In this typical preparation process, bismuth-bromine-oleylamine (Bi–Br–OA) complexes were firstly ordered over 15 d stirring and then, with slow water addition, the complexes gradually hydrolyzed and self-assembled into ultrafine nanotubes (Fig. 4(b-h)).

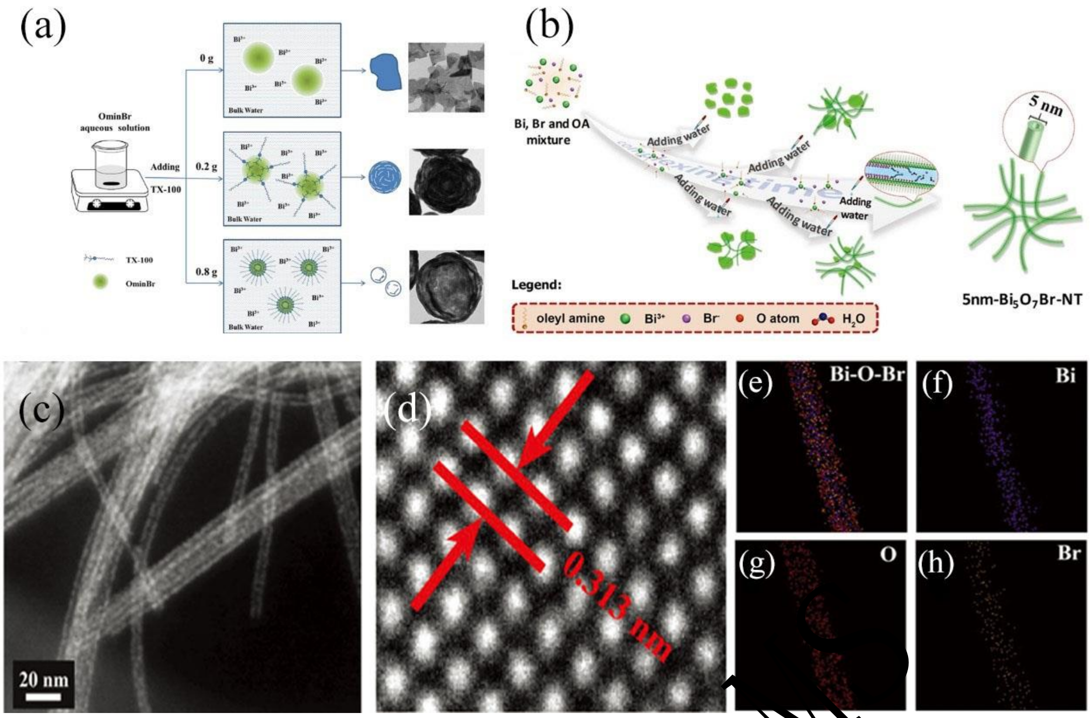

Fig. 4. Representative photocatalysts morphology formation process (a) Schematic illustration for the proposed formation process of Bi-rich $Bi_4O_5Br_2$ with different morphologies [77] (b) Schematic illustration of the preparation process of ultrafine $Bi_5O_7Br$ nanotubes [93] (c-h) HADDF-STEM-EDS mapping of Bi, O, Br elements. Reprinted with permission from Elsevier, Wiley-VCH.

## 2.3 BiOX with defect introduction

Appropriate surface defects can control the electronic states and coordination structures by the surface dangling bonds and localized electrons [94, 95]. In term of photocatalysis, defect engineering, such as OVs and metal atom vacancies, is the most effective strategies for the modulation of absorption range, charge separation, transport properties, or active sites of catalyst [96]. For example, introduction of surface metal atom defects in the ultrathin BiOCl nanosheets contributes to both up-shifted VBM and CBM, which remarkably inhibits the recombination of charge carriers [37]. The introduction of OVs usually accelerates the exciton dissociation and distorts the localization of the band-edge states, benefiting the enhanced charge-carrier generation. Especially in BiOX, the typical layer structure and the long bond-length and low bond-energy of the Bi–O bond might be beneficial to the formation of OVs in BiOX [27, 97]. The typical layer structure of BiOX makes it possible for the exposed O atoms to escape from surface to form vacancies. Then the localized electronic states (consisting of the Bi 6p orbital) appeared at the position lower than the CB minimum and thus form a new shallow donor levels [98-100]. Nowadays, the electron spin resonance spectra are usually employed to glean more direct evidence for the presence of oxygen vacancies. The signal at $g = 2.0001$ is a characteristic peak of OVs (Fig. 5a) [101]. Besides, Wu and coworkers also used annular bright-field STEM (ABFSTEM) images to directly visualize the OVs in BiOCl. As shown in Fig. 5b, OVs exhibited much brighter dots compared to the O atoms, which were marked as red circles [102].

In principle, the OVs on BiOX could serve as potential centers for the photogenerated electrons on CB, thus impeding the direct recombination of electron-hole pairs. Meanwhile, OVs might favor the capture of typical molecules ($O_2$, $H_2O$, $CO_2$ and $N_2$), which is beneficial for boosting the photocatalytic performance on the surface of BiOX [103, 104]. The OVs-mediated molecule adsorption is supposed to promote electron-transfer rate due to strong coupling. For example, OVs-mediated photocatalysis realize sustainable molecular oxygen activation, conquering the spin forbidden reactions of $O_2$ in triplet state. Therefore, oxidants (such as $O_2$) can directly generate reactive oxygen species (ROS) to degrade pollutants.

Owing to these improved activities, numerous studies have reported that enriched OVs in BiOX could extend light response to long wavelength to visible light. In general, BiOCl with the band gap around 3.3 eV exhibits only UV light absorption ability, while the incorporation of OVs gave rise to the visible light driven photocatalytic activity [105]. As illustrated in Fig. 5c, Xie and co-workers synthesized two types of BiOCl samples (nanoplates and nanosheets). With the thickness of BiOCl nanosheets reduced from 30 nm to atomic level (thickness of ~2.7 nm), the type of vacancies changes from $V'''_{Bi}$ to $V'''_{Bi}V^{\bullet\bullet}_{O}V'''_{Bi}$ vacancy associates, apparently narrowing the band energy of BiOCl from 3.25 eV to 3.00 eV. Besides, formation of OVs on BiOI nanosheets also gave rise to a red shift of ~100 nm in the light absorption band and a magnitude promotion in donor density, as well as a significant promotion in photocatalytic degradation of MO [106].

Very recently, it has been found that OVs have an impact on the involved excitonic process, thus enhancing photocatalytic selectivity and conversion for organic synthesis [107-109]. Employing OVs-mediated BiOBr as a model material, it has been reported that oxygen vacancy introduction effectively transforms excitons to charge carriers, thus accelerating benzylamine compounds undergo a smooth oxidation to N-benzylidene benzylamine [96]. Commonly, femtosecond time-resolved transient absorption spectra act as a robust indicator for the photogenerated charge concentration in BiOX systems. As illustrated in Fig. 5d, OVs-mediated BiOBr exhibits a much stronger intensity, which means a longer photoinduced electrons recovery average lifetime compared to pristine BiOBr. The longer average electrons lifetime brought about effective $\bullet O_2^-$ production and then realized excellent photocatalytic performance of imines synthesis from amines, with over 90% conversion and selectivity. Interestingly, similar results were also observed for OVs-mediated BiOCl, which further found that the photocatalytic activity was partially dependent on the levels of oxygen vacancies [110].

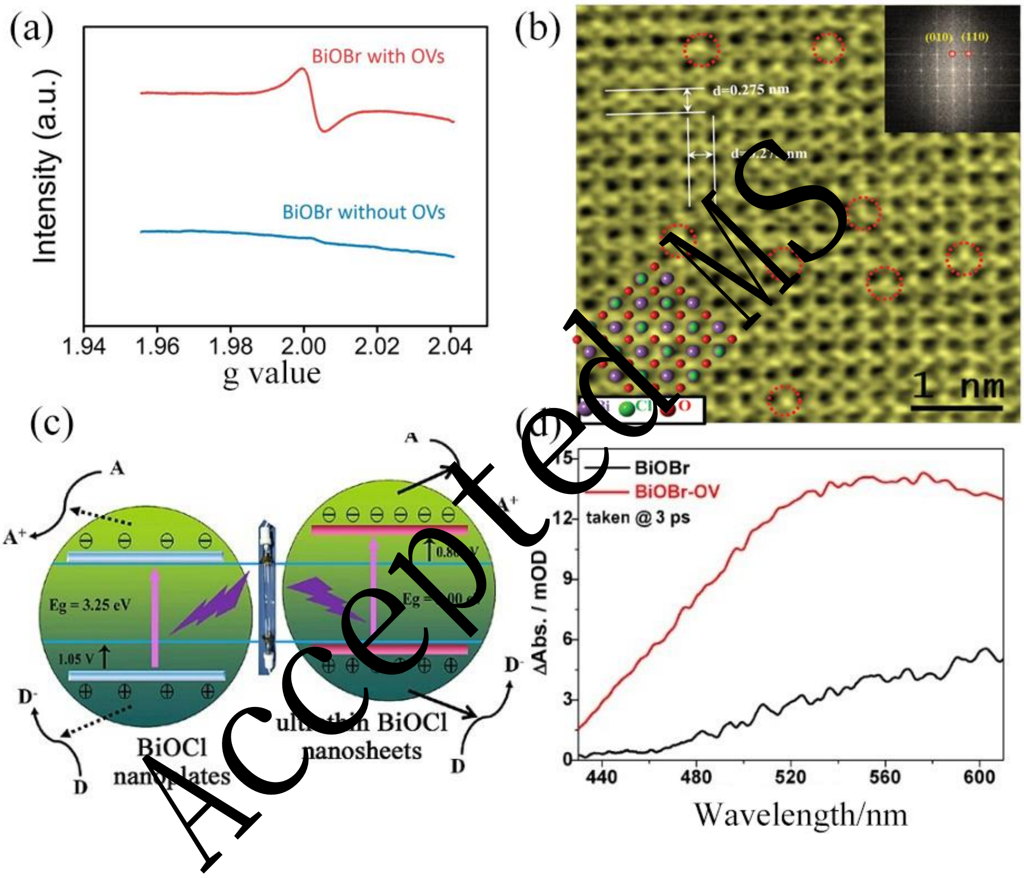

Fig. 5. (a) Low-temperature EPR spectra of BiOBr with and without OVs. [111]; (b) ABF-STEM images of UV-BiOCl-OH samples and FFT patterns with some example OVs noted by red circles (c) Schematic illustration of the band structure of ultrathin BiOCl nanosheets and BiOCl nanoplates, the upshifting of valence band maximum, and conduction band minimum effectively separate the photoinduced electron−hole pairs in ultrathin BiOCl nanosheets [37]. (d) Representative TA spectra taken at the probe delay of 3 ps for both samples [96]. Reprinted with permission from American Chemical Society.

Similar to OVs-$TiO_2$, approaches such as elevated temperatures, light irradiation, and high volts of scanning tunneling microscope contributed to oxygen vacancy introduction in BiOX. Typically, the involvement of lattice oxygen in the driven synthesis reaction can result in oxygen deficiency on the surface of BiOX [105, 107, 112]. For example, during the solvothermal and hydrothermal process, the alcohol groups of ethylene glycol, mannitol and glycerol can react with the oxygen exposed on the facets surfaces of BiOX to eliminate surface hydroxyl groups, thus constructing surface vacancy. The annealing pure BiOX at raised temperatures (generally >200 $^{o}$C) under pure $N_2$/Ar gas atmosphere or vacuum condition is also a usual method to form oxygen vacancies. For example, Wang and Yong [96] have obtained BiOBr-OV by calcining under vacuum conditions and the OVs could lead to instability production of excitons production by partly distorting the band-edge states around the defective sites. On the contrary, heating BiOCl-OV [113] in $O_2$ atmosphere under 300 ℃ condition for 4 h could prepare defect-free BiOCl.

Moreover, oxygen vacancies can also be created by ultrasonic stripping and lithium-intercalation process. For instance, $Bi_{12}O_{17}Cl_2$ nanosheets were immersed in n-butyllithium solvent in argon atmosphere to keep heating 100 $^{o}$C for 72 h and after sonicated for 40 min it would be rich in surface oxygen vacancies. Organic ligands in n-butyllithium and lattice oxygen atoms on $Bi_{12}O_{17}Cl_2$ would strongly interact with each other to construct coordinate bonds in this condition. During a long time ultrasonication exfoliation procedure, the bond fission of organic ligands would spontaneously generate oxygen vacancies on surface of single-layered $Bi_{12}O_{17}Cl_2$

nanosheets [114].

However, it's worth noting that the position of OVs can be partly filled with coupled molecules during photocatalytic process. Therefore, the stability and regeneration of surface OVs need in-depth study. Fortunately, photo-induced process may open up a new avenue for designing easily regenerated OVs to deeply understand defect-dependent surface characteristics. Recently, Li et al. [115] has observed the OVs generation on BiOCl under the UV light. Accordingly, under ambient UV light conditions, the photo-induced electrons are trapped by molecular oxygen, while holes are trapped at the surface lattice O along the (001) direction to partially neutralize the O anions. Then the trapped holes partly weaken the binding bond between localized Bi atom and the lattice oxygen, and thus in favor of the removal of surface O atoms. Obviously, this surface structure is highly favor of the OV generation through $(O–O)^{4-} + 4h^+ \rightarrow O_2$ reaction, releasing $O_2$ and accomplishing the final step for the OV formation. Therefore, the long-term photocatalytic stability and efficiency are rooted in the OVs on the 001 faces of BiOCl refreshed by UV light.

### 2.4 Element doping

Element doping, including both metal doping and non-metal doping, is a common approach for tailoring the absorption edges of Bi-based materials [32]. This method usually achieves perfect visible-light absorption and sufficient active species production for photocatalysts [116, 117]. To date, metallic elements (e.g. Ti, Fe, Mn, Co and rare earth elements) [118-123] and non-metallic elements (e.g. C, N, S and I) [124-127] doping into BiOX both have been widely reported. Commonly, option of doping element is a vital process basing on two central criteria: (1) The doping elements could capture electron/hole and conduce to their local separation; (2) Release of electron/hole is essential for subsequent migration process to the interface [54].

Transition metal doping is an efficient strategy for BiOX, as it affects the band structure, inhibits the recombination of electron-hole pairs and prolongs the life of the carriers. For example, Jiang and co-workers [128] demonstrated that Ag/Ti-doped BiOBr, Ti-doped BiOBr and Fe-doped BiOBr could be prepared via a facile one-pot solvothermal method and applied to RhB removal. Comparably, the hollow Fe-doped BiOBr showed the highest RhB degradation ability, which was attributed to the tune of the bandgap and the formation of the hollow structure with Fe doping. Recently, Wang et al. reported that Co-doping could extend the light absorption region and enhance the charge transportation efficiency by forming a doping energy level in the band gap of BiOCl [121]. No significant variation of VB maximum (2.39 eV) and CB minimum (-0.70 eV) was observed in Co-BiOCl, whereas an additional energy level constructing of Co 3d orbitals and a little O 2p orbital appeared as the mid-gap state. The position of the additional energy level is calculated to be 1.19 eV, which is responsible for the red-shift of absorption edge and promotion of electron-hole pairs. Subsequently, trivalent rare-earth ions-doping have attracted increasing interest due to their low-toxic nature and good activated luminescence properties for the host lattice of bismuth oxyhalides.

Compared to metallic doped BiOX, non-metal ion doping not only plays a role in the valence band position tailoring, but also acts as an IEF tuner. Lin et al. [129] demonstrated that the I-doped BiOBr could modulate valence band through the formation of consecutive $I^-$ impurity levels. Besides, the FI-IR spectra of B-doped BiOBr [126] exhibited the enriched surface hydroxyl groups, which efficiently promoted the absorption of pollutant. More importantly, the non-metal ion doping, which acts as an IEF tuner to efficiently improve bulk-charge separation was also investigated. Taking C-doped $Bi_3O_4Cl$ as an example, its IEF was proportional to the concentrations of carbon dopants [56]. And the $Bi_3O_4Cl$ with carbon concentration of 3.16% possessed the highest IEF, which is 126 times than $Bi_3O_4Cl$ (Fig. 6a). Meanwhile, the femtosecond-resolved transient absorption spectroscopy (TAS) was used to probe the electron transfer dynamics. As shown in Fig. 6b, C-doped $Bi_3O_4Cl$ remained 60% of the maximum electrons alive after 4000 ps charge decay. This remarkably extended electrons lifetime evidently demonstrated the fast separation of electron-hole pairs in C-doped $Bi_3O_4Cl$, which can be ascribed to the ultrastrong IEF.

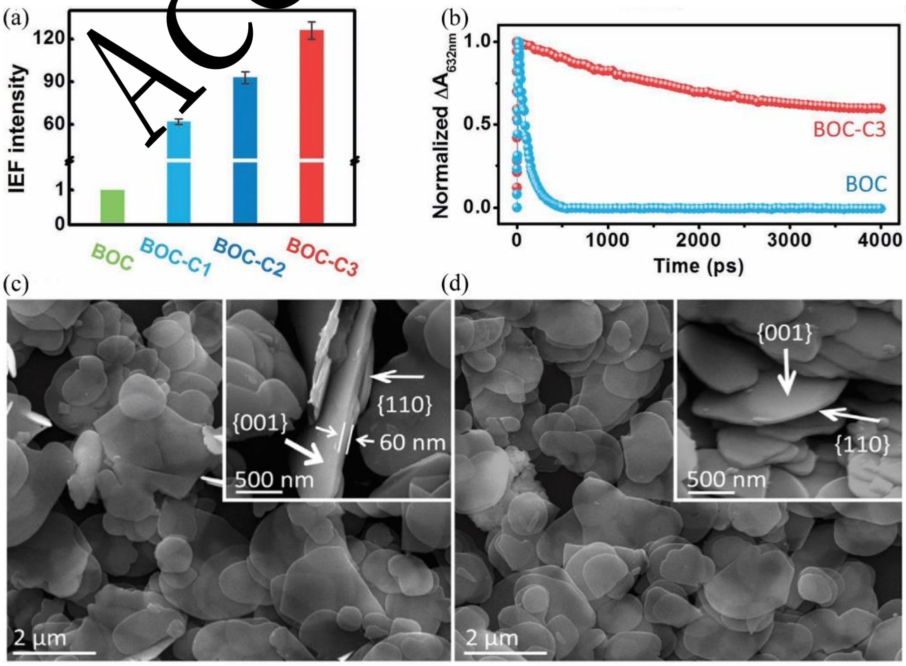

Fig. 6. (a) Variation in IEF intensity of C-doped $Bi_3O_4Cl$, BOC- $Bi_3O_4Cl$, BOC-C1-0.92%C doped $Bi_3O_4Cl$, BOC-C2-1.86% C doped $Bi_3O_4Cl$, BOC-C3-3.16% C doped $Bi_3O_4Cl$. (b) PL spectra of pure and C-doped $Bi_3O_4Cl$, and$Bi_3O_4Cl$ with various surface/interface modifications [56]. (c) the pristine BiOI, (d) In-2 BiOI [123].

To date, various methods have been exploited for the preparation of element-doped BiOX (Table 1). Among these methods, hydro-/solvothermal routes are extensively and deeply investigated. For example, Li et al. [123] adopted a facile one-shot solvothermal method via mixing $Bi(NO_3)_3$ $5H_2O$, KI and $In(NO_3)_3$ and keeping at 160 °C for 2 h to synthesize In-doped BiOI. As a result, In-doped BiOI nanosheets with the thickness of 60 nm were obtained and promoted photocatalytic activity towards p-chloroaniline (PCA) under visible light irradiation, which was about 10 times faster than that of untreated BiOI.

In addition to conventional one-shot solvothermal procedure, a homogenous carbon doping in BiOCl was successfully synthesized by a two-step pre-hydrothermal carbonization processing and subsequent calcination treatment [124]. The initial hydrothermal process induced dopant precursor of carbonaceous nanoclusters into the shallow lattice of BiOCl. Then, the calcination treatment in air brought the diffusion of carbon dopant from the home position toward the host lattice atom. Through time-dependent X-ray photoelectron spectroscopy (XPS) analysis to decode incorporation of carbon dopants into their lattices and UV-vis diffuse reflection spectra to directly image the absorption range, they demonstrated that the homogeneous carbon doping efficiently lifted the VBM and extended light-response range.

## 2.5 Other methods

### 2.5.1 Heterojunction

Heterojunction structure, exhibiting coupling interaction between two or more semiconductors with well-matched band structures, has been regard as an efficient structure for meliorating the separation of photogenerated charge carries and the visible light harvesting [130]. Such a heterogeneous system is endowed with interacted surfaces and the robust synergistic effect [131]. For this reason, construction of heterojunctions by coupling BiOX with other semiconductors has been expected to be effective in enhancing its photocatalytic capacity. To date, the coupled semiconductors include BiOX [73, 132-137], other Bi-based nanomaterials [138-141], metal oxides [142-144], organic semiconductors [145-148] and others [149-151].

Based on the type of electron-hole pair migration and separation, the BiOX-based heterojunction could be classified into conventional and Z-scheme heterojunctions. The three different carrier migrations are illustrated in Fig. 7. Nowadays, the studies of BiOX-based heterojunction are mainly focused on the type II junction and Z-scheme systems. In convention II junction, the electrons transfer from the CB of semiconductor a (SC-a) to the CB of semiconductor b while the holes transfer from the VB of semiconductor b (SC-b) to the VB of SC-a. This is because that the CB and VB levels of SC-b is lower than the CB and VB levels of SC-a. Thus far, use of convention II junction has been recognized as an efficient strategy for building a huge potential gradient and electron field to induce efficient charge separation. For example, BiOI@$Bi_{12}O_{17}Cl_2$ [111] was synthesized by simple in situ glycol-assisted assembling BiOI on the surface of $Bi_{12}O_{17}Cl_2$ nanosheets. The high-efficiency separation and transfer of electron and holes, resulting from the BiOI 001 active facets and convention II junction of BiOI@$Bi_{12}O_{17}Cl_2$, was identified as the main reasons for enhanced photocatalytic activity for degradation of RhB and 2,4-dichlorophenol. Similar to BiOI@$Bi_{12}O_{17}Cl_2$, a series of heterojunctions such as $Bi_2WO_6$-BiOCl [139], BiOBr/$Bi_2WO_6$ [140], $BiPO_4$-$BiOCl_xBr_{1-x}$ [141] have reported this type of electron-hole pair migration and separation. Conversely, in a Z-scheme system, the photo-excited electrons in the CB of SC-a will transfer to the VB of SC-b and recombine with photo-excited holes. As a result, the holes and electrons will remain in the VB of SC-a and CB of SC-b, respectively, which efficiently promote the separation of electrons-holes and maximize the redox ability of BiOX-based heterojunction.

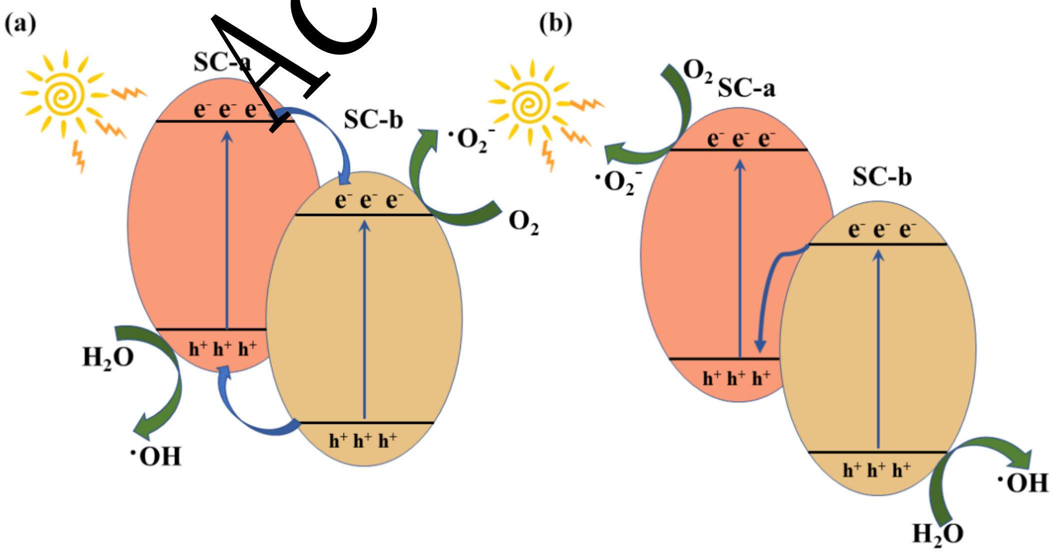

Fig. 7. Schematic representation of photogenerated electron-hole separation mechanism on (a)

type II junction and (b) direct Z-scheme systems.

### 2.5.2 Facet effect

In general, single-crystalline material can present different electronic structures to obtain distinctive photocatalytic properties through the proportion adjustment of different facets [65, 166]. Ye et al. firstly prepared BiOCl nanosheets with dominant (001) facets in 2011 and reported that the enhanced photoactivity was related to the formation of oxygen vacancies [27]. Lately, (001) BiOI with oxygen defect [111] has been reported, which exhibited excellent photocatalytic activity for the degradation of HCHO. The enhanced photocatalytic performance could be attributed to the high (001) facets and the introduction of oxygen vacancies, thus efficient promoting the separation and migration of charge carriers. Moreover, BiOBr nanosheets [153] with fully exposed (001) facets possess efficient photocatalytic performance for bacterial inactivation due to the assistance of oxygen vacancies.

The other strategies using facets effects are to tune internal electric field [110, 154]. As mentioned above, Zhang's group detailly investigated the facet effects of BiOCl and reported a correlation relationship between the facet exposure and internal electric field (IEF). It was demonstrated that the exposed 001 facets efficiently utilize IEF to promote the separation of electron-hole pairs. As a result, the enhanced IEF yields higher photoreactivity. In their subsequent work of single-crystal $Bi_3O_4Cl$ [155], they synthesized 86%, 91%, 95% 001 faceted $Bi_3O_4Cl$ and measured the corresponding magnitude variation of IEF to further clarify the effect of facets. It is found that the more 001 facets exposed on the surface of $Bi_3O_4Cl$, the stronger IEF was measured.

### 2.5.3 Surface plasmonic resonance

As an optical phenomenon, plasmonic photocatalysis depending on the combination of semiconductor and metal (e.g., gold, silver and bismuth) has received wide attention. Two characteristic features: (I) Schottky junctions and (II) localized surface plasmon resonances (LSPRs) endow plasmonic photocatalysts with preferable photoreactivity. The Schottky barrier between metal and the interface of the semiconductors, which drives photo-induced charge carriers around this area to migrate in opposite directions. Simultaneously, the LSPRs phenomenon results in a strong resonant optical absorption [156]. Recently, similar to Ag and Au nanoparticles, Bi elements had been found to exhibit a direct plasmonic photocatalytic performance [157-159]. Hong et al. [160] fabricated 3D sunflower-like $BiOCl_xI_{1-x}$ with Bi nanoparticles and surface disorders by using $NaBH_4$ as a suitable reductant at room temperature. The Bi nanoparticles on surface of $BiOCl_xI_{1-x}$ could act as electron scavengers promoting electron-hole pair separation, which greatly improve the visible-light-driven photocatalytic performance for dyes and phenols degradation. In another case, Dong et al. [161] formed Bi metal @oxygen-defective BiOCl via one-step solvothermal method, exhibiting superior photocatalytic activity for NOx removal. Through in-situ FITR spectra to decode OVs-mediated reaction intermediates, they demonstrated that (I) the NO could be adsorbed on the surface of BiOCl and then oxidized to virous forms of nitrite and nitrate; (II) the OVs on the surface of BiOCl ensure the transition of electron-hole pairs under visible light illumination and Bi nanoparticles could transfer more hot electrons to adsorbed $O_2$ to increase the production of $\bullet O_2^-$ radicals.

### 2.5.4 Strain engineering

In recent studies, strain engineering has been a well-established technique to modify electronic band structures and construct a lateral pseudo-heterostructure [162, 163]. Feng et al. synthesized square and circular BiOBr by pH modulation in 2015 and realized that the different morphologies generated different inner strains, thus impacting the band symmetry [164]. Fig. 8 shows the TEM and geometric phase analysis based on HRTEM images of square and circular BiOBr. Although both of the samples are 2D materials, the internal strain distributions of BiOBr-circle are smaller and more uniform than BiOBr-square. Therefore, even though the circular morphology has a narrower light absorption spectra and smaller surface area than those of square geometry, the former exhibited a more excellent photocatalytic performance in the photodegradation of pollutants.

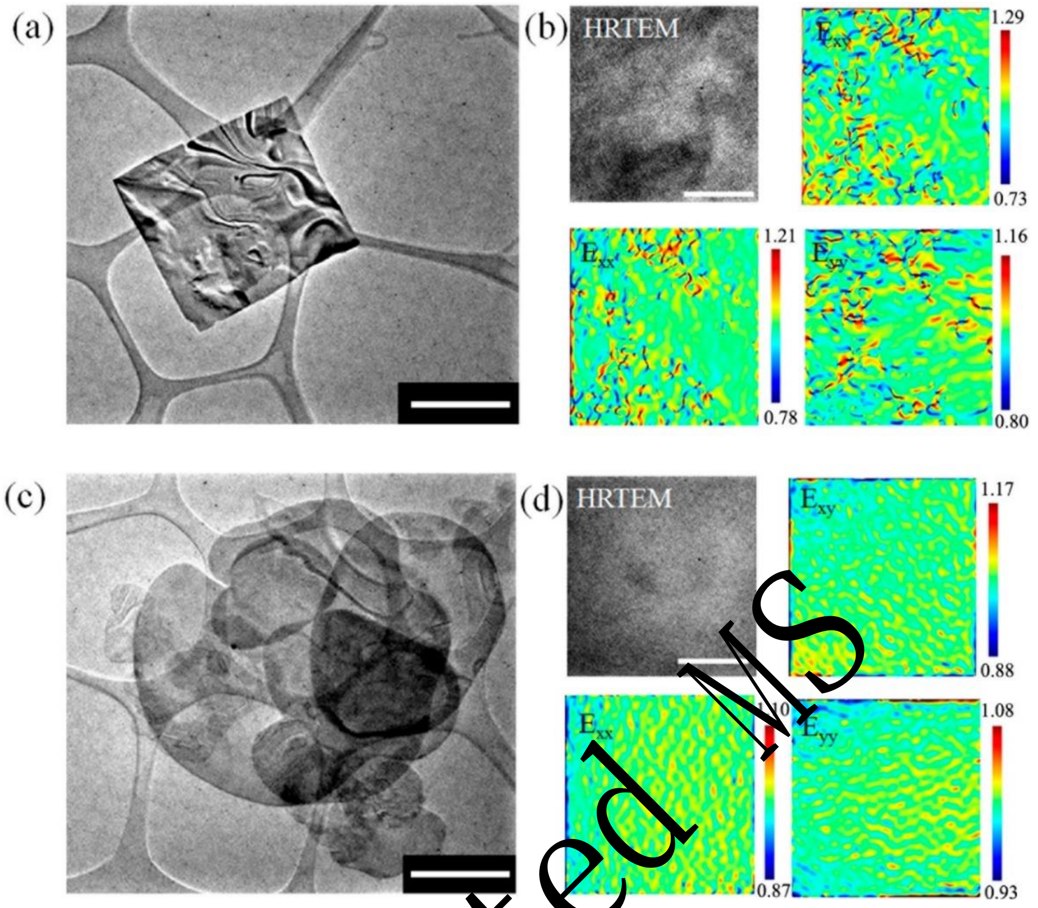

Fig. 8. TEM images of (a) BiOBr-square and (c) BiOBr-circle (scale bars are 1000 nm). Strain simulation of (b) BiOBr-square and (d) BiOBr-circle based on HRTEM (scale bars are 10 nm). The internal strain distributions are in the xy-direction ($E_{xy}$), the x-direction ($E_{xx}$), and the y direction ($E_{yy}$), with the scale for the whole image area [164]. Reprinted with permission from The Royal Society of Chemistry. Reprinted with permission from American Chemical Society.

## 4 Photocatalysis environment application of BiOX

Environment remediation is one of intense studied topics that we are facing today in photocatalysis field. Motivated by the enormous demand to solve pollution problems, much effort has been made to explore new catalysts to achieve green degradation of pollutants [47, 112, 178, 179]. It is clear that quite a number of BiOX with engineering layered structure have been investigated as promising photocatalysts to ideally attain good photocatalytic performance. In this section, we try to give a systematic summary on the current photocatalysis application of BiOX, ranging from the degradation of aquatic pollutants to air purification.

## 4.1 Degradation of aquatic pollutants

Various pollutants, such as dye, antibiotics, phenols and heavy metals, existed widely in water, which seriously influence public health and ruin global ecosystem [107, 177, 180-182]. Hence, there is a growing interest in photocatalytic degradation of contaminants in water [183-185]. The redox reactions between BiOX and aquatic pollutants are dependent on the free radicals produced by electrons or holes. Based on the controllable structural design of the synthesis, it is easy to construct BiOX with desirable capacity to absorb light, thereby initiating tailorable photocatalytic properties for the application in this topic.

In general, the photocatalysis procedure of dyes includes both degradation and detoxification [186-188]. Motivated by the discovery of BiOX as effective photocatalysts, a series of BiOX with engineering layered structure have been used to degrade different organic dyes, like methylene blue (MB), methyl orange (MO) and RhB [189]. Recently, Wang et al. [85] found the degradation rate of MO was related to concentration of OVs on the surface of BiOBr, which was about 5.3 times than that of pristine BiOBr. Interestingly, through active species trapping experiments, holes were the dominating oxidative species, but $\bullet O_2^-$ could obviously boost photocatalytic performance. A possible explanation was that the adsorbed $O_2$ on the OVs acted as a trap for electrons, thus enhancing the separation of charge carriers. Moreover, the photocatalytic degradation performance of MB by BiOCl-OVs was also been explored by Bhawna Sarwan and co-workers [173]. It was proposed that electrons could transfer from the VB to OV states under visible light. Meanwhile, OVs was an active electron traps, resulting in the efficient separation of the hole-electron pairs. Consequently, the degradation rates of gray BiOCl (BiOCl-OVs) was 4.72 times as fast as that of pristine BiOCl.

The strategy to synthesize alloyed BiOX is a conventional method used for dye degradation. Theoretical calculations [190] first revealed that solid solutions represented a precise manipulation of the CB and VB level, achieving an optimal balance between the wider of the absorption spectrum and more adequate redox potential. Based on this point, in order to find a correlation between the tunable band position and reaction potential of the valence band, Ren and his coworkers [191] synthesized $BiOM_xR_{1-x}$ (M, R = Cl, Br, I) photocatalysts by precipitating at a low-temperature and the optimized alloyed BiOX ($BiOCl_{0.5}Br_{0.5}$, $BiOCl_{0.75}I_{0.25}$ and $BiOBr_{0.75}I_{0.25}$ ) exhibited the highest photocatalytic performance for the degradation of RhB. Then, it has also been reported that solid solutions could enhance movement/distribution of photogenerated free carriers because of the impurity defects acting as trap centers for free carriers [21]. Compared with pure BiOX, alloyed BiOX generally possess smaller nanosheets and larger surface areas, and it is easier to self-assemble 3D hierarchical flower-like nanostructures during growth process [60]. Therefore, besides the aforementioned 3D flowerlike $BiOCl_{0.875}Br_{0.125}$ [64] which can completely decomposed 15 mg/L RhB solution within 120 s upon visible light and kept the decomposition progression even after turning off the light source in the course of the process (after 40 s), RhB solution ($2 \times 10^{-5}$ mol/L) could also be totally decomposed in 6 min by using 5% $WO_3$-$BiOCl_{0.25}Br_{0.75}$ photocatalysts (0.5 g $L^{-1}$) under visible-light irradiation [192].

As a worldwide used medicine in diseases and agricultural production, antibiotics are hazardous to ecosystem due to their inherent toxicity and persistence in environment [193, 194]. Based on the multiple engineering of layered structure, it is easy to construct BiOX with tailorable photocatalytic activity to degrade different antibiotics, such as tetracycline (TC), ciprofloxacin (CIP) and 4-methylaminoantipyrine (4-MMA). To evaluate the degradation and mineralization of antibiotics during photocatalytic process of BiOX, a series of technologies have been extensively adopted. The classical mineralization index is defined as removing ratio of total organic carbon (TOC). For instance, after 60 min of visible light irradiation, $Bi_{24}O_{31}Br_{10}$ nanoflakes [69] eliminated 70.9% of the TOC, showing a remarked mineralization ability to TC. Lately, considering autofluorescence properties of TC, 3D excitation−emission spectra (EEMs) combined with high-performance liquid−mass spectrometry (HPLC−MS) were used for exploring its mineralization properties. The intensity of fluorescence during photodegrading TC obviously changed with the reaction time, indicating the degradation of low-molecular organic compounds by CCN/$Bi_{12}O_{17}Cl_2$ [195].

BiOX has exhibited excellent performance for the photodegradation of phenols into low-molecular organic compounds and inorganic $CO_2$, $H_2O$, $NO_2^-$, $NO_3^-$ etc. [196, 197]. It was observed that $Bi_{12}O_{15}Cl_6$ [85] exhibited excellent photocatalytic activity for the degradation of bisphenol A under visible-light illumination (BPA, a representative endocrine-disrupting pollutant), corresponding to 13.6 times as high as that of BiOCl. The favorable rich of [Bi-O] layers brought about suitable energy band structure and thus produced $h^+$, •OH, and $•O_2^-$ to participate in the oxidation reaction during photocatalysis. The detailed reactions process was displayed as follows.

$$Bi_{12}O_{15}Cl_6 + hv \rightarrow h^+ + e^- \tag{11}$$

$$O_2 + e^- \rightarrow •O_2^- \tag{12}$$

$$•O_2^- + •O_2^- + 2H^+ \rightarrow H_2O_2 + O_2 \tag{13}$$

$$H_2O_2 + e^- \rightarrow •OH + OH^- \tag{14}$$

$$BPA + h^+, •O_2^- \text{ or } •OH \rightarrow \text{degradation products} \tag{15}$$

The interchange-center role of oxygen-vacancy-mediated and bismuth-rich-mediated photocatalysis in the degradation of antibiotics and phenols are also elucidated in detail in this review. To form a Z-scheme system, $BiO_{1-x}Br/Bi_2O_2CO_3$ [145] was prepared by adjusting the process parameter such as the concentration of NaBr and reaction time. The difference between two different photocatalytic systems is shown in Fig. 9. Comparably, the Z-scheme photocatalyst exhibits highly enhanced apparent photocatalytic rate constant of per unit surface area for BPA up to $13.24 \times 10^{-3}\ m^{-2}\ h^{-1}$ and 4- MMA to $15.53 \times 10^{-3}\ m^{-2}\ h^{-1}$($k/S_{BET}$) under visible light irradiation, which is respectively 3.2 times and 6.6 times than that of non-oxygen vacancy involved $BiO_{1-x}Br/Bi_2O_2CO_3$ photocatalysts system. In this Z-scheme system, oxygen vacancies act as electron mediator or storage center of photogenerated electron-hole pairs, thus achieving excellent production efficiency of active species (Fig. 9a). These findings have greatly promoted the process of practical application for BiOX in wastewater remediation.

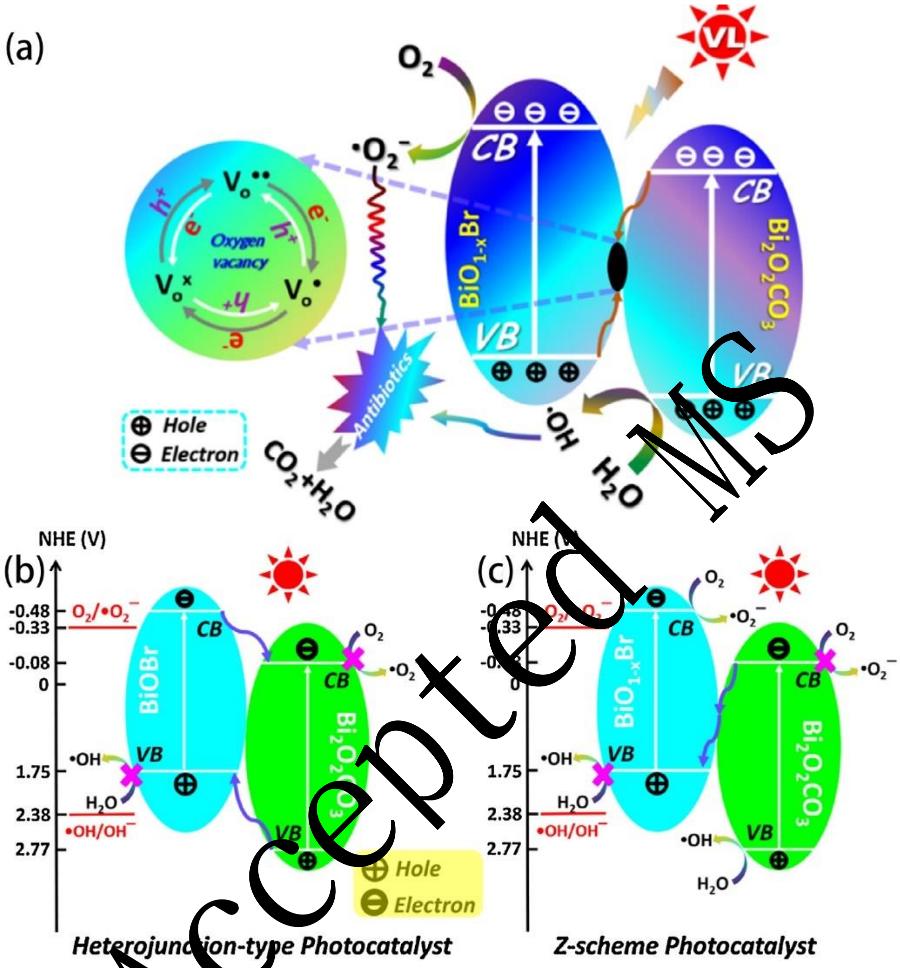

Fig. 9. Schematic illustration of two different photocatalytic systems and photocatalytic mechanisms. (a) Illustration of photocatalytic mechanisms of Z-scheme $BiO_{1-x}Br/Bi_2O_2CO_3$ [159]. Schematic illustration of two different photocatalytic systems: (b) heterojunction-type and (c) Z-scheme mechanisms photocatalytic system [145]. Reprinted with permission from Elsevier.

### 3.2 Air purification

Nitrogen monoxide (NOx) is one of the most usual gaseous pollutants, which leads to various atmospheric environmental problems including acid rain, photochemical smog and so on [198]. The degradation of the gaseous pollutants via photocatalysis is mainly comprised of three crucial steps: (I) charge separation and transportation; (II) the formation of $\bullet O_2^-$ species or $\bullet OH$ ; (III) catalytic reduction reactions [199]. In fact, a series of BiOX photocatalysts of bismuth-rich and alloying have been employed in photoreduction of $NO_x$. The photocatalytic activity of 3D flower-like $BiOCl_xBr_{1-x}$ [166] was expounded by oxidizing NO at 100 ppb levels under visible light illumination (λ> 400 nm). During the photoreduction process, 0.2g $BiOCl_{0.5}Br_{0.5}$ was dispersed into a diameter of 10 cm dish and showed satisfying photocatalytic activity. This was mainly due to the fact that 3D flower-like structure offered large surface area and the solid solution modified the band gap to adopt the optimized balance between the enhanced visible light adsorption and adequate redox potentials. In general, combination of OVs and construction of heterojunctions in BiOX can lead to better photocatalytic performance. For example, Zhao et al. [200] formed BiOCl/ppy -OVs by a room temperature chemical method. According to in situ diffuse reflectance infrared Fourier-transform spectroscopy and radical trapping experiments, the OVs acted as active site to efficiently adsorb and active $O_2$ molecular which remarkably increase the production of $\bullet O_2^-$. As a result, the NO was inclined to be oxidized into $NO_3^-$ instead of $NO_2$ under the high concentration of $\bullet O_2^-$. This photocatalytic process offers an efficient strategy to simultaneously inhibit toxic intermediates and enhance photocatalytic activity.

$SO_2$ emitted from the burning of sulfur-containing fossil fuels for domestic heating, power generation and motor vehicles are main factors of sulfuric acid formation, which is the main component of acid rain. Compared to NOx, the application of BiOX as photoreduction of $SO_2$ are much less. Inspired by BiOI/$Al_2O_3$-padded trickling scrubber system [201], in which $SO_2$ and NO can be totally reduced by the visible light irradiation at the same time, the use of BiOX to achieve photoreduction of $SO_2$ still need further research.

Similar to photoreduction of NOx, the severe environmental hazards of volatile organic compounds (VOCs) have took great enthusiasm in the environmental applications of BiOX. Recently, a novel group of $BiO(ClBr)_{(1-x)/2}I_x$ solid solutions with visible light absorption were synthesized and achieved a precisely control of band gaps ranging from 2.88 to 1.82 eV [202]. As illustrated in Fig. 10, $BiO(ClBr)_{0.375}I_{0.25}$ showed the maximum efficiency in $CO_2$ evolution, which was 2.3 and 23.2 times higher than $BiO(ClBr)_{0.5}$ and BiOI, respectively. Nevertheless, $BiO(ClBr)_{0.21}I_{0.58}$ performs best in the acetone evolution (215.6 μmol•$h^{-1}$•$g^{-1}$). To further investigate the reaction mechanism, a fluorescence method was used to measure the photocatalytic generation of •OH. The photo-induced holes of $BiO(ClBr)_{0.5}$ could react with $H_2O$ to form •OH radicals because the VBM (+ 2.88eV vs. NHE) is more positive than that of •OH /$H_2O$ (+2.80eV vs. NHE). However, the substitution of Cl and Br by I lead to upshifts of the VBM, thus $BiO(ClBr)_{(1-x)/2}I_x$ was more likely directly oxidized IPA by photoinduced holes (Fig. 10c). In addition, it has also been reported that (001) BiOI with oxygen defects represent superior photocatalytic activity for the removal of formaldehyde gas [111]. This distinct enhancement was due to the fact that the introduced oxygen defects efficiently promote the separation and transport of photoinduced electron-hole pairs. This work provided a novel strategy to fabricate BiOX-based materials for the removal of formaldehyde gas using facet and oxygen defects.

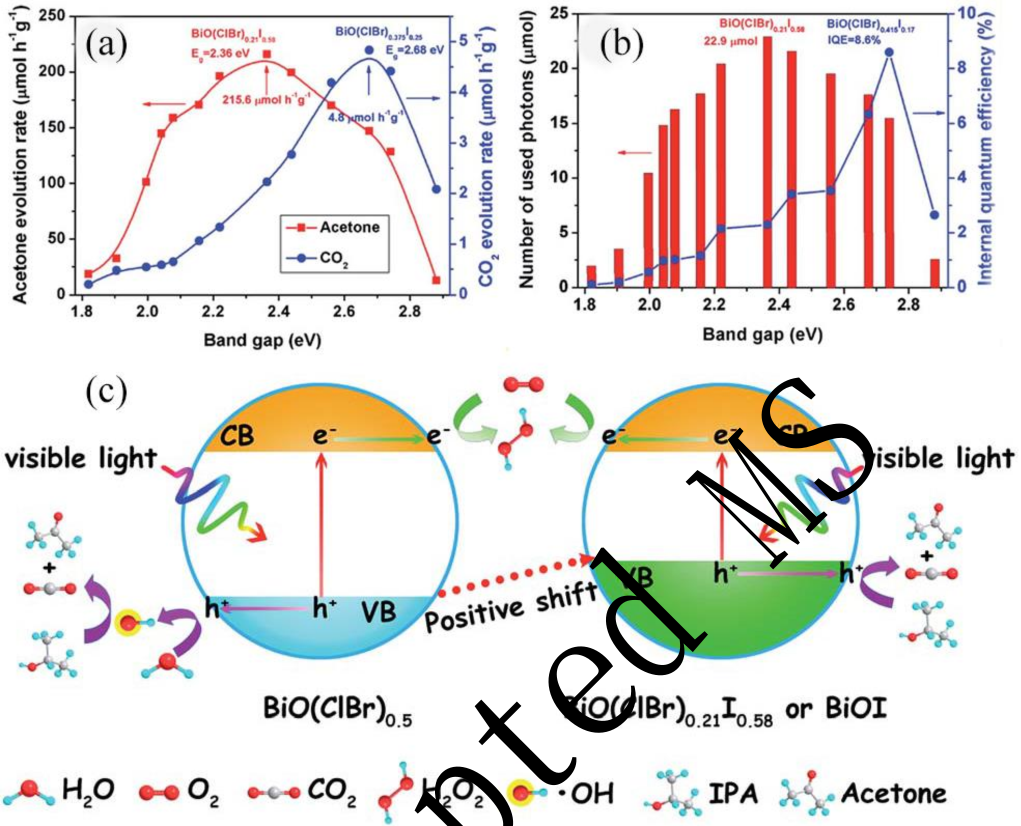

Fig. 10. (a) Evolution rates of acetone and $CO_2$, and (b) number of used photons (in one hour) and internal quantum efficiencies as the functions of band gap in $BiO(ClBr)_{(1-x)/2}I_x$ solid solutions. (c) Proposed mechanism of photo oxidizing IPA over BiO $(ClBr)_{(1-x)/2}I_x$ solid solutions [202]. Reprinted with permission from The Royal Society of Chemistry.

## 5 Summary and outlook

The unique layered structure and tunable electronic structure endow BiOX photocatalysts with excellent photocatalytic activity and promising application for environmental remediation. However, pristine BiOX suffered from inherent drawbacks, including poor light absorption, lack of surface-active sites, and rapid recombination possibility for the electron-holes. To address environment challenge, multiply structural optimized strategies have opened a new possibility to improve the photocatalytic performance. In this review, we have highlighted recent advances in the fabrication of BiOX in controllable performance and their potential environment applications. The synthetic section firstly imparted the exhaustive demonstration of the photochemical properties and synthesis methods of alloyed, bismuth-rich, doped and defect-introduced BiOX. Besides, the introduction of heterojunction, facet effect, surface plasmonic resonance and strain engineering can also improve the photocatalytic activity of BiOX. Emerging research has demonstrated BiOX-based nanomaterials to be an efficient photocatalyst for photodegradation of aquatic pollutants and air purification. Despite much advancement in this area has been obtained as outlined above, there are still several difficulties that limit the wide usage of BiOX. Below are some prospective opportunities for future study:

The limited performance in environment remediation can be, in part attributed to synthesis challenges in design of BiOX-based materials. Current studies reveal that reducing layered materials to monolayers or ultrathin nanosheets is beneficial for the migration of photoinduced charge carries and the exposed atoms escaping from a lattice to construct vacancies. More BiOX-based materials with atomic thickness should be extensively synthesized to full explore their potential.

Although some effort has been developed to construction of alloyed BiOX, the alloyed type is almost based on pristine BiOX. The mix-and-match strategies among alloying, bismuth-rich strategy, defect introduction is rarely investigated in detail. Previous studies have demonstrated that bismuth-rich strategies provide a perfect platform to investigate IEF. Element doping and facet control are available approaches for the enhancement of IEF. More efficient strategies such as construction of homojunction and reducing thickness need further exploration. In addition, the introduction of surface OVs in BiOX is an efficient modulation strategy to extend light absorption and accelerate separation of charge carries. However, the study of other types of defect appearing in BiOX such as halogen vacancies and dual vacancies is still lacking. Further research should pay attention to the formation of other types of defects and specific mechanism of photocatalysis under the different types of defects.

The improved characterization can develop new insight into clarifying the evolution of structure and detailly understanding photocatalytic process. Nowadays, current characterization is usually based on ex-situ methods. Photochemical-reaction mechanism exploration under in-situ reaction conditions is instructive to prepare high-performance photocatalysts. One promising in situ technique is in-situ TEM, which provides new potential in exploring advanced materials based on the structure-property correlativity. Recently in situ TEM have been developed to observe the photocatalytic splitting of water and growth of nanowires to clarify the reaction pathways [203, 204]. These techniques could offer fundamental structural information on the BiOX and their stability under reaction conditions, which would turn into input for constructing relevant model structure in DFT calculation.

BiOX remains a unique layered material with excellent photochemical properties that have potential to be significantly developed in various environment application. However, most of BiOX-based photodegradation are evaluated in aqueous solutions.

For gaseous pollutants especially VOCs, the relative reports are much insufficient. Simultaneously, the toxic monitoring of photocatalytic system during the treatment of complex organic pollutants should be developed to prevent secondary pollution. At last, hopefully in this review we have partly lifted the mysterious veil of structure-property correlativity based on the full understanding of distinct electronic and optical properties of BiOX-based materials, thus promoting and advancing the various applications of bismuth-based photocatalysts.

**Acknowledgements**

This work was supported by the National Natural Science Foundation of China (No. 51508177, 51709101, 51579098, 51779090), the National Program for Support of Top–Notch Young Professionals of China (2014), China Postdoctoral Science Foundation (2017M610498), Hunan Provincial Science and Technology Plan Project (No.2016RS3026, 2017SK2243), and the Program for Changjiang Scholars and Innovative Research Team in University (IRT-13R17)

## References

[1] P. Xu, G.M. Zeng, D.L. Huang, C.L. Feng, S. Hu, M.H. Zhao, C. Lai, Z. Wei, C. Huang, G.X. Xie, Z.F. Liu, Use of iron oxide nanomaterials in wastewater treatment: A review, Sci. Total Environ., 424 (2012) 1-10.

[2] X. Ren, G. Zeng, L. Tang, J. Wang, J. Wan, Y. Liu, J. Yu, H. Yi, S. Ye, R. Deng, Sorption, transport and biodegradation - An insight into bioavailability of persistent organic pollutants in soil, Sci. Total Environ., 610 (2018) 1154-1163.

[3] C. Zhou, C. Lai, C. Zhang, G. Zeng, D. Huang, M. Cheng, L. Hu, W. Xiong, M. Chen, J. Wang, Y. Yang, L. Jiang, Semiconductor/boron nitride composites: Synthesis, properties, and photocatalysis applications, Appl. Catal. B: Environ., 238 (2018) 6-18.

[4] H. Yi, D. Huang, L. Qin, G. Zeng, C. Lai, M. Cheng, S. Ye, B. Song, X. Ren, X. Guo, Selective prepared carbon nanomaterials for advanced photocatalytic application in environmental pollutant treatment and hydrogen production, Appl. Catal. B: Environ., 239 (2018) 408-424.

[5] L. Armelao, D. Barreca, G. Bottaro, A. Gasparotto, C. Maccato, C. Maragno, E. Tondello, U.L. Štangar, M. Bergant, D. Mahne, Photocatalytic and antibacterial activity of $TiO_2$ and Au/$TiO_2$ nanosystems, Nanotechnology, 18 (2007) 375709.

[6] A. Šuligoj, U.L. Štangar, A. Ristić, M. Mazaj, D. Verhovšek, N.N. Tušar, $TiO_2$–$SiO_2$ films from organic-free colloidal $TiO_2$ anatase nanoparticles as photocatalyst for removal of volatile organic compounds from indoor air, Appl. Catal. B: Environ., 184 (2016) 119-131.

[7] Y. Yang, C. Zhang, C. Lai, G. Zeng, D. Huang, M. Cheng, J. Wang, F. Chen, C. Zhou, W. Xiong, BiOX (X = Cl, Br, I) photocatalytic nanomaterials: Applications for fuels and environmental management, Adv. Colloid. Interfac., 254 (2018) 76-93.

[8] A. Kudo, Y. Miseki, Heterogeneous photocatalyst materials for water splitting, Chem. Soc. Rev., 38 (2009) 253-278.

[9] S.C. Roy, O.K. Varghese, M. Paulose, C.A. Grimes, Toward solar fuels: photocatalytic conversion of carbon dioxide to hydrocarbons, Acs Nano 4 (2010) 1259-1278.

[10] M.R. Hoffmann, S.T. Martin, W. Choi, D.W. Bahnemann, Environmental applications of semiconductor photocatalysis, Chem. Rev. 95 (1995) 69-96.

[11] Z. Cai, A.D. Dwivedi, W.N. Lee, X. Zhao, W. Liu, M. Sillanpää, D. Zhao, C.H. Huang, J. Fu, Application of nanotechnologies for removing pharmaceutically active compounds from water: development and future trends, Environ. Sci-Nano., (2017) 27-47.

[12] X. Gong, D. Huang, Y. Liu, G. Zeng, R. Wang, J. Wan, C. Zhang, M. Cheng, X. Qin, W. Xue, Stabilized Nanoscale Zerovalent Iron Mediated Cadmium Accumulation and Oxidative Damage of Boehmeria nivea (L.) Gaudich Cultivated in Cadmium Contaminated Sediments, Environ. Sci. Technol., 51 (2017) 11308-11316

[13] D. Huang, R. Deng, J. Wan, G. Zeng, W. Xue, X. Wen, C. Zhou, L. Hu, X. Liu, P. Xu, Remediation of lead-contaminated sediment by biochar-supported nano-chlorapatite: Accompanied with the change of available phosphorus and organic matters, J. Hazar. Mater., 348 (2018) 109-116

[14] J.M. Bothwell, S.W. Krabbe, R.S. Mohan, Applications of bismuth(III) compounds in organic synthesis, Chem. Soc. Rev., 40 (2011) 4649-4707.

[15] J. Wang, L. Tang, G. Zeng, Y. Deng, H. Dong, Y. Liu, L. Wang, B. Peng, C. Zhang, F. Chen, 0D/2D Interface Engineering of Carbon Quantum Dots Modified $Bi_2WO_6$ Ultrathin Nanosheets with Enhanced Photoactivity for Full Spectrum Light Utilization and Mechanism Insight, Appl. Catal. B: Environ., 222 (2018) 115-123.

[16] L. Jiang, X. Yuan, G. Zeng, J. Liang, X. Chen, H. Yu, H. Wang, Z. Wu, J. Zhang, T. Xiong, In-situ synthesis of direct solid-state dual Z-scheme $WO_3$/g-$C_3N_4$/$Bi_2O_3$ photocatalyst for the degradation of refractory pollutant, Appl. Catal. B: Environ., 227 (2018) 376-385.

[17] H. Wang, X. Yuan, Y. Wu, G. Zeng, W. Tu, C. Sheng, Y. Deng, F. Chen, W.C. Jia, Plasmonic Bi nanoparticles and BiOCl sheets as cocatalyst deposited on perovskite-type $ZnSn(OH)_6$ microparticle with facet-oriented polyhedron for improved visible-light-driven photocatalysis, Appl. Catal. B: Environ., 209 (2017) 543-553.

[18] Z. Ran, X. Wang, Y. Li, D. Yang, X.-G. Zhao, K. Biswas, D.J. Singh, L. Zhang, Bismuth and antimony-based oxyhalides and chalcohalides as potential optoelectronic materials, NPJ. Comput. Mater., 4 (2018) UNSP 14.

[19] K. Zhang, C. Liu, F. Huang, C. Zheng, W. Wang, Study of the electronic structure and photocatalytic activity of the BiOCl photocatalyst, Appl. Catal. B: Environ., 68 (2006) 125-129.

[20] Q.C. Liu, D.K. Ma, Y.Y. Hu, Y.W. Zeng, S.M. Huang, Various bismuth oxyiodide hierarchical architectures: alcohothermal-controlled synthesis, photocatalytic activities, and adsorption capabilities for phosphate in water, ACS Appl. Mater. Inter., 5 (2013) 11927-11934.

[21] X. Zhang, L. Zhang, Electronic and band structure tuning of ternary semiconductor photocatalysts by self doping: the case of BiOI, J. Phys. Chem. C., 114 (2010) 18198-18206.

[22] J. Jiang, K. Zhao, X. Xiao, L. Zhang, Synthesis and facet-dependent photoreactivity of BiOCl single-crystalline nanosheets, J. Am. Chem. Soc., 134 (2012) 4473-4476.

[23] A. Fujishima, K. Honda, Electrochemical Photolysis of Water at a Semiconductor Electrode, Nature, 238 (1972) 37-38.

[24] X. Zhang, Z. Ai, F. Jia, L. Zhang, Generalized one-pot synthesis, characterization, and

photocatalytic activity of hierarchical BiOX (X = Cl, Br, I) nanoplate microspheres, J. Phys. Chem. C., 112 (2008) 747-753.

[25] S. Wu, C. Wang, Y. Cui, T. Wang, B. Huang, X. Zhang, X. Qin, P. Brault, Synthesis and photocatalytic properties of BiOCl nanowire arrays, Mater. Lett., 64 (2010) 115-118.

[26] J. Xiong, G. Cheng, G. Li, F. Qin, R. Chen, Well-crystallized square-like 2D BiOCl nanoplates: mannitol-assisted hydrothermal synthesis and improved visible-light-driven photocatalytic performance, RSC Adv., 1 (2011) 1542-1553

[27] L. Ye, L. Zan, L. Tian, T. Peng, J. Zhang, The {001} facets-dependent high photoactivity of BiOCl nanosheets, Chem. Commun., (Camb) 47 (2011) 6951-6953.

[28] J. Xia, J. Zhang, S. Yin, H. Li, H. Xu, L. Xu, Q. Zhang, Advanced visible light photocatalytic properties of BiOCl micro/nanospheres synthesized via reactable ionic liquids, J. Phys. Chem. Solids., 74 (2013) 298-304.

[29] B. Zhang, G. Ji, M.A. Gondal, Y. Liu, X. Zhang, X. Chang, N. Li, Rapid adsorption properties of flower-like BiOI nanoplates synthesized via a simple EG-assisted solvothermal process, J. Nanopart. Res., 15 (2013) UNSP 1773

[30] K. Li, Y. Tang, Y. Xu, Y. Wang, Y. Huo, H. Li, J. Jia, A BiOCl film synthesis from $Bi_2O_3$ film and its UV and visible light photocatalytic activity, Appl. Catal. B: Environ., 140-141 (2013) 179-188.

[31] N.T. Hahn, S. Hoang, J.L. Self, C.B. Mullins, Spray pyrolysis deposition and photoelectrochemical properties of n-Type BiOI nanoplatelet thin films, ACS Nano, (2012) 7712-7722.

[32] H. Tong, S. Ouyang, Y. Bi, N. Umezawa, M. Oshikiri, J. Ye, Nano-photocatalytic materials: possibilities and challenges, Adv. Mater., 24 (2012) 229-251.

[33] X. Gao, G. Tang, W. Peng, Q. Guo, Y. Luo, Surprise in the phosphate modification of BiOCl with

oxygen vacancy: In situ construction of hierarchical Z-scheme BiOCl-OV-$BiPO_4$ photocatalyst for the degradation of carbamazepine, Chem. Eng. J., 360 (2019) 1320-1329.

[34] H. Fallahi Motlagh, M. Haghighi, M. Shabani, Sono-solvothermal fabrication of ball-flowerlike $Bi_2O_7Sn_2$-$Bi_7O_9I_3$ nanophotocatalyst with efficient solar-light-driven activity for degradation of antibiotic tetracycline, Solar Energy 180 (2019) 25-38.

[35] C. Liu, J. Zhou, J. Su, L. Guo, Turning the unwanted surface bismuth enrichment to favourable $BiVO_4$/BiOCl heterojunction for enhanced photoelectrochemical performance, Appl. Catal. B: Environ., 241 (2019) 506-513.

[36] M. Shabani, M. Haghighi, D. Kahforoushan, A. Haghighi, Sono-solvothermal hybrid fabrication of BiOCl-$Bi_{24}O_{31}Cl_{10}$/rGO nano-heterostructure photocatalyst with efficient solar-light-driven performance in degradation of fluoroquinolone antibiotics, Sol. Energ. Mat. Sol. C., 193 (2019) 335-350.

[37] M. Guan, C. Xiao, J. Zhang, S. Fan, R. An, Q. Cheng, J. Xie, M. Zhou, B. Ye, Y. Xie, Vacancy associates promoting solar-driven photocatalytic activity of ultrathin bismuth oxychloride nanosheets, J. Am. Chem. Soc., 135 (2013) 10411-10417.

[38] X. Zhang, B. Li, J. Wang, Y. Yuan, Q. Zhang, Z. Gao, L.M. Liu, L. Chen, The stabilities and electronic structures of single-layer bismuth oxyhalides for photocatalytic water splitting, Phys. Chem. Chem. Phys., 16 (2014) 25854-25861.

[39] W.L. Huang, Q. Zhu, DFT calculations on the electronic structures of BiOX (X = F, Cl, Br, I) photocatalysts with and without semicore Bi 5d states, J. Comput. Chem., 30 (2009) 183-190.

[40] W. Wang, P. Xu, M. Chen, G. Zeng, C. Zhang, C. Zhou, Y. Yang, D. Huang, C. Lai, M. Cheng, L. Hu, W. Xiong, H. Guo, M. Zhou, Alkali Metal-Assisted Synthesis of Graphite Carbon Nitride with

Tunable Band-Gap for Enhanced Visible-Light-Driven Photocatalytic Performance, ACS Sus. Chem. Eng., 6 (2018) 15503-15516.

[41] D. Voiry, H.S. Shin, K.P. Loh, M. Chhowalla, Low-dimensional catalysts for hydrogen evolution and $CO_2$ reduction, Nat. Rev. Chem. 2 (2018) UNSP 0105

[42] N. Hazari, Homogeneous iron complexes for the conversion of dinitrogen into ammonia and hydrazine, Chem. Soc. Rev., 39 (2010) 4044-4056.

[43] J. Li, H. Li, G. Zhan, L. Zhang, Solar Water Splitting and Nitrogen Fixation with Layered Bismuth Oxyhalides, Accounts. Chem. Res., 50 (2016) 112.

[44] L. Wang, D. Lv, Z. Yue, H. Zhu, L. Wang, D. Wang, X. Xu, W. Hao, S.X. Dou, Y. Du, Promoting photoreduction properties via synergetic utilization between plasmonic effect and highly active facet of BiOCl, Nano Energy 57 (2019) 398-404.

[45] J. Rashid, A. Abbas, L.C. Chang, A. Iqbal, I.U. Haq, A. Rehman, S.U. Awan, M. Arshad, M. Rafique, M.A. Barakat, Butterfly cluster like lamellar BiOBr/$TiO_2$ nanocomposite for enhanced sunlight photocatalytic mineralization of aqueous ciprofloxacin, Sci. Total Environ., 665 (2019) 668-677.

[46] X.M. Sun, J. Wu, Q.Z. Liu, F.G. Tian, Mechanism insights into the enhanced activity and stability of hierarchical bismuth oxyiodide microspheres with selectively exposed (001) or (110) facets for photocatalytic oxidation of gaseous mercury, Appl. Surf. Sci., 455 (2018) 864-875.

[47] L. Ye, Y. Su, X. Jin, H. Xie, C. Zhang, Recent advances in BiOX (X = Cl, Br and I) photocatalysts: synthesis, modification, facet effects and mechanisms, Environmental Science: Nano 1 (2014) 90-112.

[48] M. Li, H. Huang, S. Yu, N. Tian, Y. Zhang, Facet, Junction and Electric Field Engineering of Bismuth-Based Materials for Photocatalysis, Chemcatchem 10 (2018) 4477-4496.

[49] Y. Yang, C. Zhang, C. Lai, G. Zeng, D. Huang, M. Cheng, J. Wang, F. Chen, C. Zhou, W. Xiong, BiOX (X = Cl, Br, I) photocatalytic nanomaterials: Applications for fuels and environmental management, Adv. Colloid. Interfac., 254 (2018) 76-93.

[50] H. Cheng, B. Huang, Y. Dai, Engineering BiOX (X = Cl, Br, I) nanostructures for highly efficient photocatalytic applications, Nanoscale 6 (2014) 2009-2026.

[51] J. Li, Y. Yu, L. Zhang, Bismuth oxyhalide nanomaterials: layered structures meet photocatalysis, Nanoscale 6 (2014) 8473-8488.

[52] H. Li, J. Li, Z. Ai, F. Jia, L. Zhang, Oxygen Vacancy-Mediated Photocatalysis of BiOCl: Reactivity, Selectivity and Perspective, Angew. Chem. Int. Edit., (2018) 122-138.

[53] R. He, D. Xu, B. Cheng, J. Yu, W. Ho, Review on nanoscale Bi-based photocatalysts, Nanoscale Horiz., 3 (2018) 464-504.

[54] J. Di, J. Xia, H. Li, S. Guo, S. Dai, Bismuth oxyhalide layered materials for energy and environmental applications, Nano Energy 41 (2017) 172-192.

[55] X. Jin, L. Ye, H. Xie, G. Chen, Bismuth-rich bismuth oxyhalides for environmental and energy photocatalysis, Coordin. Chem. Rev., 349 (2017) 84-101.

[56] J. Li, L. Cai, J. Shang, Y. Yu, L. Zhang, Giant Enhancement of Internal Electric Field Boosting Bulk Charge Separation for Photocatalysis, Adv. Mater., 28 (2016) 4059-4064.

[57] Z. He, P. Alexandridis, Ionic liquid and nanoparticle hybrid systems: Emerging applications, Adv. Colloid. Interfac., 244 (2017) 54-70.

[58] Structure-dependent photocatalytic performance of $BiOBr_xI_{1-x}$ nanoplate solid solutions, Catalysts 7 (2017) 153.

[59] H. Zhang, L. Liu, Z. Zhou, Towards better photocatalysts: first-principles studies of the alloying

effects on the photocatalytic activities of bismuth oxyhalides under visible light, Phys. Chem. Chem. Phys., 14 (2012) 1286-1292.

[60] Y. Liu, W.J. Son, J. Lu, B. Huang, Y. Dai, M.H. Whangbo, Composition dependence of the photocatalytic activities of $BiOCl_{(1-x)}Br_{(x)}$ solid solutions under visible light, Chemistry 17 (2011) 9342-9349.

[61] S. Ouyang, J. Ye, beta-$AgAl_{(1-x)}Ga_{(x)}O_2$ solid-solution photocatalysts: continuous modulation of electronic structure toward high-performance visible-light photoactivity, J. Am. Chem. Soc., 133 (2011) 7757-7763.

[62] Q. Wang, Z. Liu, D. Liu, G. Liu, M. Yang, F. Cui, W. Wang, Ultrathin two-dimensional $BiOBr_xI_{1-x}$ solid solution with rich oxygen vacancies for enhanced visible-light-driven photoactivity in environmental remediation, Appl. Catal. B: Environ., 236 (2018) 222-232.

[63] S. Shenawi-Khalil, V. Uvarov, Y. Kritsman, E. Menes, I. Popov, Y. Sasson, A new family of $BiO(Cl_xBr_{1-x})$ visible light sensitive photocatalysts, Catal. Commun., 12 (2011) 1136-1141.

[64] H. Gnayem, Y. Sasson, Hierarchical Nanostructured 3D Flowerlike $BiOCl_xBr_{1-x}$ Semiconductors with Exceptional Visible Light Photocatalytic Activity, ACS Catal., 3 (2013) 186-191.

[65] J. Yang, Y. Liang, K. Li, Y. Zhu, S. Liu, R. Xu, W. Zhou, Design of 3D flowerlike $BiOCl_xBr_{1-x}$ nanostructure with high surface area for visible light photocatalytic activities, J. Alloys Compd., 725 (2017) 1144-1157.

[66] Z. Liu, J. Niu, P. Feng, Y. Zhu, Solvothermal synthesis of $Bi_{24}O_{31}Cl_xBr_{10-x}$ solid solutions with enhanced visible light photocatalytic property, Ceram. Int., 41 (2015) 4608-4615.

[67] X. Xiao, C. Liu, R. Hu, X. Zuo, J. Nan, L. Li, L. Wang, Oxygen-rich bismuth oxyhalides: generalized one-pot synthesis, band structures and visible-light photocatalytic properties, J. Mater.

Chem., 22 (2012) 22840-22843.

[68] N. Umezawa, O. Shuxin, J. Ye, Theoretical study of high photocatalytic performance of $Ag_3PO_4$, Physical Review B 83 (2011) 035202.

[69] X. Xiao, R. Hu, C. Liu, C. Xing, X. Zuo, J. Nan, L. Wang, Facile microwave synthesis of novel hierarchical $Bi_{24}O_{31}Br_{10}$ nanoflakes with excellent visible light photocatalytic performance for the degradation of tetracycline hydrochloride, Chem. Eng. J., 225 (2013) 790-797.

[70] H. Huang, K. Xiao, T. Zhang, F. Dong, Y. Zhang, Rational design on 3D hierarchical bismuth oxyiodides via in situ self-template phase transformation and phase-junction construction for optimizing photocatalysis against diverse contaminants, Appl. Catal. B: Environ., 203 (2017) 879-888.

[71] J. Shang, W. Hao, X. Lv, T. Wang, X. Wang, Y. Du, S. Dou, T. Xie, D. Wang, J. Wang, Bismuth Oxybromide with Reasonable Photocatalytic Reduction Activity under Visible Light, ACS Catal., 4 (2014) 954-961.

[72] X. Lou, J. Shang, L. Wang, H. Feng, W. Hao, T. Wang, Y. Du, Enhanced Photocatalytic Activity of $Bi_{24}O_{31}Br_{10}$: Constructing Heterojunction with BiOI, J. Mater. Sci. Technol., 33 (2017) 281-284.

[73] S. Ning, L. Ding, Z. Lin, Q. Lin, H. Zhang, H. Lin, J. Long, X. Wang, One-pot fabrication of $Bi_3O_4Cl$/BiOCl plate-on-plate heterojunction with enhanced visible-light photocatalytic activity, Appl. Catal. B: Environ., 185 (2016) 203-212.

[74] J. Xia, M. Ji, J. Di, B. Wang, S. Yin, M. He, Q. Zhang, H. Li, Improved photocatalytic activity of few-layer $Bi_4O_5I_2$ nanosheets induced by efficient charge separation and lower valence position, J. Alloys Compd., 695 (2017) 922-930.

[75] X. Jin, L. Ye, H. Wang, Y. Su, H. Xie, Z. Zhong, H. Zhang, Bismuth-rich strategy induced photocatalytic molecular oxygen activation properties of bismuth oxyhalogen: The case of $Bi_{24}O_{31}Cl_{10}$,

Appl. Catal. B: Environ., 165 (2015) 668-675.

[76] J. Wang, Y. Yu, L. Zhang, Highly efficient photocatalytic removal of sodium pentachlorophenate with $Bi_3O_4Br$ under visible light, Appl. Catal. B: Environ., 136-137 (2013) 112-121.

[77] D. Mao, S. Ding, L. Meng, Y. Dai, C. Sun, S. Yang, H. He, One-pot microemulsion-mediated synthesis of Bi-rich $Bi_4O_5Br_2$ with controllable morphologies and excellent visible-light photocatalytic removal of pollutants, Appl. Catal. B: Environ., 207 (2017) 153-165.

[78] X. Xiong, T. Zhou, X. Liu, S. Ding, J. Hu, Surfactant-mediated synthesis of single-crystalline $Bi_3O_4Br$ nanorings with enhanced photocatalytic activity, J. Mater. Chem. A, 5 (2017) 15706-15713.

[79] Z. Liu, J. Liu, Z. Liu, J. Niu, P. Feng, Soluble starch-modulated solvothermal synthesis of grain-like $Bi_{24}O_{31}Br_{10}$ hierarchical architectures with enhanced photocatalytic activity, Mater. Res. Bull., 81 (2016) 119-126.

[80] C.-Y. Wang, X. Zhang, H.-B. Qiu, G.-X. Huang, H.-Q. Yu, $Bi_{24}O_{31}Br_{10}$ nanosheets with controllable thickness for visible–light–driven catalytic degradation of tetracycline hydrochloride, Appl. Catal. B: Environ., 205 (2017) 615-623.

[81] X. Xiao, C. Xing, G. He, X. Zuo, J. Nan, L. Wang, Solvothermal synthesis of novel hierarchical $Bi_4O_5I_2$ nanoflakes with highly visible light photocatalytic performance for the degradation of 4-tert-butylphenol, Appl. Catal. B: Environ., 148-149 (2014) 154-163.

[82] S. Sun, W. Wang, L. Zhang, L. Zhou, W. Yin, M. Shang, Visible light-induced efficient contaminant removal by $Bi_5O_7I$, Environ. Sci. Technol., 43 (2009) 2005-2010.

[83] C. Zheng, G. He, X. Xiao, M. Lu, H. Zhong, X. Zuo, J. Nan, Selective photocatalytic oxidation of benzyl alcohol into benzaldehyde with high selectivity and conversion ratio over $Bi_4O_5Br_2$ nanoflakes under blue LED irradiation, Appl. Catal. B: Environ., 205 (2017) 201-210.

[84] X. Xiao, R. Hao, X. Zuo, J. Nan, L. Li, W. Zhang, Microwave-assisted synthesis of hierarchical $Bi_7O_9I_3$ microsheets for efficient photocatalytic degradation of bisphenol-A under visible light irradiation, Chem. Eng. J., 209 (2012) 293-300.

[85] C.Y. Wang, X. Zhang, X.N. Song, W.K. Wang, H.Q. Yu, Novel $Bi_{12}O_{15}Cl_6$ Photocatalyst for the Degradation of Bisphenol A under Visible-Light Irradiation, ACS Appl. Mater. Inter., 8 (2016) 5320-5326.

[86] P. Cui, J. Wang, Z. Wang, J. Chen, X. Xing, L. Wang, R. Yu, Bismuth oxychloride hollow microspheres with high visible light photocatalytic activity, Nano Res., 9 (2016) 593-601.

[87] L. Ye, X. Jin, C. Liu, C. Ding, H. Xie, K.H. Chu, P.K. Wong, Thickness-ultrathin and bismuth-rich strategies for BiOBr to enhance photoreduction of $CO_2$ into solar fuels, Appl. Catal. B: Environ., 187 (2016) 281-290.

[88] Y. Bai, T. Chen, P. Wang, L. Wang, L. Ye, Bismuth-rich $Bi_4O_5X_2$ (X = Br, and I) nanosheets with dominant {1 0 1} facets exposure for photocatalytic $H_2$ evolution, Chem. Eng. J., 304 (2016) 454-460.

[89] C. Ding, L. Ye, Q. Zhao, Z. Zhong, K. Liu, H. Xie, K. Bao, X. Zhang, Z. Huang, Synthesis of $Bi_xO_yI_z$ from molecular precursor and selective photoreduction of $CO_2$ into CO, J. $CO_2$. Util., 14 (2016) 135-142.

[90] Y. Su, H. Wang, L. Ye, X. Jin, H. Xie, C. He, K. Bao, Shape-dependent photocatalytic activity of $Bi_5O_7I$ caused by facets synergetic and internal electric field effects, RSC Adv. 4 (2014) 65056-65064.

[91] J. Wang, Y. Li, Synthesis of single-crystalline nanobelts of ternary bismuth oxide bromide with different compositions, Chem. Commun., (2003) 2320-2321.

[92] X. Lin, T. Huang, F. Huang, W. Wang, J. Shi, Photocatalytic activity of a Bi-based oxychloride $Bi_3O_4Cl$, J. Phys. Chem. B., 110 (2006) 24629-24634.

[93] S. Wang, X. Hai, X. Ding, K. Chang, Y. Xiang, X. Meng, Z. Yang, H. Chen, J. Ye, Light-Switchable Oxygen Vacancies in Ultrafine $Bi_5O_7Br$ Nanotubes for Boosting Solar-Driven Nitrogen Fixation in Pure Water, Adv. Mater., 29 (2017) 1701774.

[94] X. Pan, M.Q. Yang, X. Fu, N. Zhang, Y.J. Xu, Defective $TiO_2$ with oxygen vacancies: synthesis, properties and photocatalytic applications, Nanoscale 5 (2013) 3601-3614.

[95] K. Lai, W. Wei, Y. Zhu, M. Guo, Y. Dai, B. Huang, Effects of oxygen vacancy and N-doping on the electronic and photocatalytic properties of $Bi_2MO_6$ (M=Mo, W), J. Solid. State. Chem., 187 (2012) 103-108.

[96] H. Wang, D. Yong, S. Chen, S. Jiang, X. Zhang, W. Shao, Q. Zhang, W. Yan, B. Pan, Y. Xie, Oxygen-Vacancy-Mediated Exciton Dissociation in BiOBr for Boosting Charge-Carrier-Involved Molecular Oxygen Activation, J. Am. Chem. Soc., 140 (2018) 1760-1766.

[97] L. Ye, K. Deng, F. Xu, L. Tian, T. Peng, L. Zan, Increasing visible-light absorption for photocatalysis with black BiOCl, Phys. Chem. Chem. Phys., 14 (2012) 82-85.

[98] X. Zhang, L. Zhao, C. Fan, Z. Liang, P. Han, Effects of oxygen vacancy on the electronic structure and absorption spectra of bismuth oxychloride, Comp. Mater. Sci., 61 (2012) 180-184.

[99] X. Zhang, C. Fan, Y. Wang, Y. Wang, Z. Liang, P. Han, DFT+U predictions: The effect of oxygen vacancy on the structural, electronic and photocatalytic properties of Mn-doped BiOCl, Comp. Mater. Sci., 71 (2013) 135-145.

[100] D. Cui, L. Wang, K. Xu, L. Ren, L. Wang, Y. Yu, Y. Du, W. Hao, Band-gap engineering of BiOCl with oxygen vacancies for efficient photooxidation properties under visible-light irradiation, J. Mater. Chem. A., 6 (2018) 2193-2199.

[101] F.T. Li, Q. Wang, J. Ran, Y.J. Hao, X.J. Wang, D. Zhao, S.Z. Qiao, Ionic liquid self-combustion

synthesis of BiOBr/$Bi_{24}O_{31}Br_{10}$ heterojunctions with exceptional visible-light photocatalytic performances, Nanoscale 7 (2015) 1116-1126.

[102] S. Wu, J. Xiong, J. Sun, Z.D. Hood, W. Zeng, Z. Yang, L. Gu, X. Zhang, S.Z. Yang, Hydroxyl-dependent evolution of oxygen vacancies enables the regeneration of BiOCl photocatalyst, ACS Appl. Mater. Inter., 9 (2017) 16620-16626.

[103] S. Polarz, J. Strunk, V. Ischenko, M.W.E.V.D. Berg, O. Hinrichsen, M. Muhler, M. Driess, On the Role of Oxygen Defects in the Catalytic Performance of Zinc Oxide, Angew. Chem. Int. Edit., 45 (2006) 2965-2969.

[104] K. Zhao, L. Zhang, J. Wang, Q. Li, W. He, J.J. Yin, Surface structure-dependent molecular oxygen activation of BiOCl single-crystalline nanosheets, J. Am. Chem. Soc., 135 (2013) 15750-15753.

[105] L. Ye, X. Jin, Y. Leng, Y. Su, H. Xie, C. Liu, Synthesis of black ultrathin BiOCl nanosheets for efficient photocatalytic $H_2$ production under visible light irradiation, J. Power Sources., 293 (2015) 409-415.

[106] Y. Huang, H. Li, M.-S. Balogun, W. Liu, Y. Tong, X. Lu, H. Ji, Oxygen vacancy induced bismuth oxyiodide with remarkably increased visible-light absorption and superior photocatalytic performance, ACS Appl. Mater. Inter., 6 (2014) 22920-22927.

[107] Y. Wu, B. Yuan, M. Li, W.H. Zhang, Y. Liu, C. Li, Well-defined BiOCl colloidal ultrathin nanosheets: synthesis, characterization, and application in photocatalytic aerobic oxidation of secondary amines, Chem Sci., 6 (2015) 1873-1878.

[108] X. Xiao, C. Zheng, M. Lu, L. Zhang, F. Liu, X. Zuo, J. Nan, Deficient $Bi_{24}O_{31}Br_{10}$ as a highly efficient photocatalyst for selective oxidation of benzyl alcohol into benzaldehyde under blue LED

irradiation, Appl. Catal. B: Environ., 228 (2018) 142-151.

[109] F. Xie, Y. Zhang, X. He, H. Li, X. Qiu, W. Zhou, S. Huo, Z. Tang, First achieving highly selective oxidation of aliphatic alcohols to aldehydes over photocatalysts, J. Mater. Chem. A., 6 (2018) 13236-13243.

[110] C. Mao, H. Cheng, H. Tian, H. Li, W.-J. Xiao, H. Xu, J. Zhao, L. Zhang, Visible light driven selective oxidation of amines to imines with BiOCl: Does oxygen vacancy concentration matter?, Appl. Catal. B: Environ., 228 (2018) 87-96.

[111] W. Fan, H. Li, F. Zhao, X. Xiao, Y. Huang, H. Ji, Y. Tong, Boosting the photocatalytic performance of (001) BiOI: enhancing donor density and separation efficiency of photogenerated electrons and holes, Chem. Commun., (Camb) 52 (2016) 5316-5319.

[112] J. Jiang, L. Zhang, H. Li, W. He, J.J. Yin, Self-doping and surface plasmon modification induced visible light photocatalysis of BiOCl, Nanoscale 5 (2013) 10573-10581.

[113] H. Li, F. Qin, Z. Yang, X. Cui, J. Wang, L. Zhang, New reaction pathway induced by plasmon for selective benzyl alcohol oxidation on BiOCl possessing oxygen vacancies, J. Am. Chem. Soc., 139 (2017) 3513-3521.

[114] L. Jie, G. Zhan, Y. Ying, L. Zhang, Superior visible light hydrogen evolution of Janus bilayer junctions via atomic-level charge flow steering, Nat. Commun., 7 (2016) 11480.

[115] H. Li, J. Shi, K. Zhao, L. Zhang, Sustainable molecular oxygen activation with oxygen vacancies on the {001} facets of BiOCl nanosheets under solar light, Nanoscale 6 (2014) 14168-14173.

[116] W. Wang, M.O. Tadé, Z. Shao, Nitrogen-doped simple and complex oxides for photocatalysis: A review, Prog. Mater. Sci., 92 (2018) 33-63.

[117] Y. Tian, B. Chang, J. Lu, J. Fu, F. Xi, X. Dong, Hydrothermal synthesis of Graphitic Carbon

Nitride–$Bi_2WO_6$ Heterojunctions with Enhanced Visible Light Photocatalytic Activities, ACS Appl. Mater. Inter., 5 (2013) 7079-7085.

[118] X. Geng, W. Li, F. Xiao, D. Wang, L. Yang, Effect of in situ Fe(II)/Fe(III)-doping on the visible light-Fenton-like catalytic activity of Bi/BiOBr hierarchical microspheres, Catal. Sci. Technol., 7 (2017) 658-667.

[119] W.T. Li, W.Z. Huang, H. Zhou, H.Y. Yin, Y.F. Zheng, X.C. Song, Synthesis of $Zn^{2+}$ doped BiOCl hierarchical nanostructures and their exceptional visible light photocatalytic properties, J. Alloys Compd., 638 (2015) 148-154.

[120] Z.S. Liu, B.T. Wu, Y.L. Zhao, J.N. Niu, Y.B. Zhu, Solvothermal synthesis and photocatalytic activity of Al-doped BiOBr microspheres, Ceram. Int., 40 (2014) 5597-5603.

[121] C.-Y. Wang, Y.-J. Zhang, W.-K. Wang, D.-N. Pei, G.-X. Huang, J.-J. Chen, X. Zhang, H.-Q. Yu, Enhanced photocatalytic degradation of bisphenol A by Co-doped BiOCl nanosheets under visible light irradiation, Appl. Catal. B: Environ., 221 (2018) 320-328.

[122] J. Xia, M. Ji, W. Li, J. Di, H. Xu, M. He, Q. Zhang, H. Li, Synthesis of erbium ions doped BiOBr via a reactive ionic liquid with improved photocatalytic activity, Colloid. Surface. A., 489 (2016) 343-350.

[123] H. Li, Z. Yang, J. Zhang, Y. Huang, H. Ji, Y. Tong, Indium doped BiOI nanosheets: Preparation, characterization and photocatalytic degradation activity, Appl. Surf. Sci., 423 (2017) 1188-1197.

[124] J. Li, Facet-Level Mechanistic Insights into General Homogeneous Carbon Doping for Enhanced Solar-to-Hydrogen Conversion, Adv. Funct. Mater., 25 (2015) 2189-2201.

[125] X. Li, G. Jiang, Z. Wei, X. Wang, W. Chen, L. Shen, One-pot solvothermal preparation of S-doped BiOBr microspheres for efficient visible-light induced photocatalysis, MRS Commun., 3

(2013) 219-224.

[126] Z. Liu, J. Liu, H. Wang, G. Cao, J. Niu, Boron-doped bismuth oxybromide microspheres with enhanced surface hydroxyl groups: Synthesis, characterization and dramatic photocatalytic activity, J. Colloid Interface Sci. 463 (2016) 324-331.

[127] X. Jia, J. Cao, H. Lin, M. Zhang, X. Guo, S. Chen, Transforming type-I to type-II heterostructure photocatalyst via energy band engineering: A case study of I-BiOCl/I-BiOBr, Appl. Catal. B: Environ., 204 (2017) 505-514.

[128] G. Jiang, X. Wang, Z. Wei, X. Li, X. Xi, R. Hu, B. Tang, R. Wang, S. Wang, T. Wang, W. Chen, Photocatalytic properties of hierarchical structures based on Fe-doped BiOBr hollow microspheres, J. Mater. Chem. A., 1 (2013) 2406-2410.

[129] H. Lin, X. Li, J. Cao, S. Chen, Y. Chen, Novel I--doped BiOBr composites: Modulated valence bands and largely enhanced visible light phtotocatalytic activities, Catal. Commun., 49 (2014) 87-91.

[130] H. Wang, L. Zhang, Z. Chen, J. Hu, S. Li, Z. Wang, J. Liu, X. Wang, Semiconductor heterojunction photocatalysts: design, construction, and photocatalytic performances, Chem. Soc. Rev., 43 (2014) 5234-5244.

[131] J. Yang, L. Xu, C. Liu, T. Xie, Preparation and photocatalytic activity of porous $Bi_5O_7I$ nanosheets, Appl. Surf. Sci., 319 (2014) 265-271.

[132] L. Hao, H. Huang, Y. Guo, X. Du, Y. Zhang, Bismuth oxychloride homogeneous phasejunction $BiOCl/Bi_{12}O_{17}Cl_2$ with unselectively efficient photocatalytic activity and mechanism insight, Appl. Surf. Sci., 420 (2017) 303-312.

[133] C. Zhou, C. Lai, D. Huang, G. Zeng, C. Zhang, M. Cheng, L. Hu, J. Wan, W. Xiong, M. Wen, Highly porous carbon nitride by supramolecular preassembly of monomers for photocatalytic removal

of sulfamethazine under visible light driven, Appl. Catal. B: Environ., 220 (2018) 202-210.

[134] C. Zhou, C. Lai, P. Xu, G. Zeng, D. Huang, C. Zhang, M. Cheng, L. Hu, J. Wan, Y. Liu, W. Xiong, Y. Deng, M. Wen, In situ grown AgI/$Bi_{12}O_{17}Cl_2$ heterojunction photocatalysts for visible light degradation of sulfamethazine: efficiency, pathway, and mechanism, ACS Sus. Chem. Eng., 6 (2018) 4174-4184.

[135] X. Lou, J. Shang, L. Wang, H. Feng, W. Hao, T. Wang, Y. Du, Enhanced photocatalytic activity of $Bi_{24}O_{31}Br_{10}$ : Constructing heterojunction with BiOI, J. Mater. Sci. Technol., 33 (2017) 281-284.

[136] Y.R. Jiang, H.P. Lin, W.H. Chung, Y.M. Dai, W.Y. Lin, C.C. Chen, Controlled hydrothermal synthesis of $BiO_xCl_y$/$BiO_mI_n$ composites exhibiting visible-light photocatalytic degradation of crystal violet, J. Hazar. Mater., 283 (2015) 787-805.

[137] Y.-H. Lee, Y.-M. Dai, J.-Y. Fu, C.-C. Chen, A series of bismuth-oxychloride/bismuth-oxyiodide/graphene-oxide nanocomposites: Synthesis, characterization, and photcatalytic activity and mechanism, Mol. Catal., 432 (2017) 196-209.

[138] G. He, C. Xing, X. Xiao, R. Hu, X. Zuo, J. Nan, Facile synthesis of flower-like $Bi_{12}O_{17}Cl_2$/β-$Bi_2O_3$ composites with enhanced visible light photocatalytic performance for the degradation of 4-tert-butylphenol, Appl. Catal. B: Environ., 170-171 (2015) 1-9.

[139] M. Hojamberdiev, Z.C. Kadirova, E. Zahedi, D. Onna, M. Claudia Marchi, G. Zhu, N. Matsushita, M. Hasegawa, S. Aldabe Bilmes, K. Okada, Tuning the morphological structure, light absorption, and photocatalytic activity of $Bi_2WO_6$ and $Bi_2WO_6$-BiOCl through cerium doping, Arab. J. Chem., (2018).

[140] J. Hu, W. An, H. Wang, J. Geng, W. Cui, Y. Zhan, Synthesis of a hierarchical BiOBr nanodots/$Bi_2WO_6$ p–n heterostructure with enhanced photoinduced electric and photocatalytic degradation performance, RSC Adv., 6 (2016) 29554-29562.

[141] Y.L. Qi, Y.F. Zheng, X.C. Song, Synthetic adjustable energy band structure of $BiPO_4$-$BiOCl_xBr_{1-x}$ p–n heterojunctions with excellent photocatalytic activity, J. Taiwan Inst Chem. E., 77 (2017) 216-226.

[142] J. Zheng, F. Chang, M. Jiao, Q. Xu, B. Deng, X. Hu, A visible-light-driven heterojuncted composite $WO_3/Bi_{12}O_{17}Cl_2$: Synthesis, characterization, and improved photocatalytic performance, J. Colloid Interface Sci. 510 (2018) 20-31.

[143] H. Cheng, J. Wu, F. Tian, Q. Liu, X. Qi, Q. Li, W. Pan, Z. Li, J. Wei, Visible-light photocatalytic oxidation of gas-phase Hg0 by colored $TiO_2$ nanoparticle-sensitized $Bi_5O_7I$ nanorods: Enhanced interfacial charge transfer based on heterojunction, Chem. Eng. J., 360 (2019) 951-963.

[144] J.-C. Sin, C.-A. Lim, S.-M. Lam, A.R. Mohamed, H. Zeng, Facile synthesis of novel ZnO/Nd-doped BiOBr composites with boosted visible light photocatalytic degradation of phenol, Mater. Lett., 248 (2019) 20-23.

[145] J. Ding, Z. Dai, F. Qin, H. Zhao, S. Zhao, R. Chen, Z-scheme $BiO_{1-x}$ $Br/Bi_2O_2CO_3$ photocatalyst with rich oxygen vacancy as electron mediator for highly efficient degradation of antibiotics, Appl. Catal. B: Environ., 245 (2019) 281-291.

[146] H. Liu, Y. Su, Z. Chen, Z. Jin, Y. Wang, Graphene sheets grafted three-dimensional $BiOBr_{0.2}I_{0.8}$ microspheres with excellent photocatalytic activity under visible light, J. Hazar. Mater., 266 (2014) 75-83.

[147] W. Zhang, Y. Liang, Facile Synthesis of Ternary $g\text{-}C_3N_4@BiOCl/Bi_{12}O_{17}Cl_2$ Composites With Excellent Visible Light Photocatalytic Activity for NO Removal, Front. Chem., 7 (2019).

[148] S. Ding, D. Mao, S. Yang, F. Wang, L. Meng, M. Han, H. He, C. Sun, B. Xu, Graphene-analogue h-BN coupled Bi-rich $Bi_4O_5Br_2$ layered microspheres for enhanced visible-light photocatalytic activity

and mechanism insight, Appl. Catal. B: Environ., 210 (2017) 386-399.

[149] M. Ji, J. Xia, J. Di, B. Wang, S. Yin, L. Xu, J. Zhao, H. Li, Ionic liquid-assisted bidirectional regulation strategy for carbon quantum dots (CQDs)/$Bi_4O_5I_2$ nanomaterials and enhanced photocatalytic properties, J. Colloid Interface Sci., 478 (2016) 324-333.

[150] D. Wu, X. Wang, H. Wang, F. Wang, D. Wang, Z. Gao, X. Wang, F. Xu, K. Jiang, Ultrasonic-assisted synthesis of two dimensional BiOCl/$MoS_2$ with tunable band gap and fast charge separation for enhanced photocatalytic performance under visible light, J. Colloid Interface Sci., 533 (2019) 539-547.

[151] J. Gao, Y. Gao, Z. Sui, Z. Dong, S. Wang, D. Zou, Hydrothermal synthesis of BiOBr/$FeWO_4$ composite photocatalysts and their photocatalytic degradation of doxycycline, J. Alloys Compd., 732 (2018) 43-51.

[152] M. Kiskinova, Surface Structure and Reactivity: Reactions on face-centered cubic (110) metal surfaces involving adatom-induced reconstructions, Cheminform 27 (1996) 1431-1448.

[153] D. Wu, B. Wang, W. Wang, T. An, G. Li, T.W. Ng, H.Y. Yip, C. Xiong, H.K. Lee, P.K. Wong, Visible-light-driven BiOBr nanosheets for highly facet-dependent photocatalytic inactivation of Escherichia coli, J. Mater. Chem. A., 3 (2015) 15148-15155.

[154] R. Zhang, Y. Dai, Z. Lou, Z. Li, Z. Wang, Y. Yang, X. Qin, X. Zhang, B. Huang, Layered photocatalyst $Bi_2O_2[BO_2(OH)]$ nanosheets with internal polar field enhanced photocatalytic activity, CrystEngComm 16 (2014) 4931-4934.

[155] J. Li, L. Zhang, Y. Li, Y. Yu, Synthesis and internal electric field dependent photoreactivity of $Bi_3O_4Cl$ single-crystalline nanosheets with high {001} facet exposure percentages, Nanoscale 6 (2014) 167-171.

[156] J. Toudert, R. Serna, M. Jiménez de Castro, Exploring the optical potential of nano-bismuth: tunable surface plasmon resonances in the near ultraviolet-to-near infrared range, J. Phys. Chem. C., 116 (2012) 20530-20539.

[157] Y. Yu, C. Cao, H. Liu, P. Li, F. Wei, Y. Jiang, W. Song, A Bi/BiOCl heterojunction photocatalyst with enhanced electron–hole separation and excellent visible light photodegrading activity, J. Mater. Chem. A., 2 (2014) 1677-1681.

[158] C. Chang, L. Zhu, Y. Fu, X. Chu, Highly active Bi/BiOI composite synthesized by one-step reaction and its capacity to degrade bisphenol A under simulated solar light irradiation, Chem. Eng. J., 233 (2013) 305-314.

[159] F. Dong, T. Xiong, S. Yan, H. Wang, Y. Sun, Y. Zhang, H. Huang, Z. Wu, Facets and defects cooperatively promote visible light plasmonic photocatalysis with Bi nanowires@BiOCl nanosheets, J. Catal., 344 (2016) 401-410.

[160] Y. Huang, B. Long, H. Li, M.-S. Balogun, Z. Rui, Y. Tong, H. Ji, Enhancing the Photocatalytic Performance of $BiOCl_xI_{1-x}$by Introducing Surface Disorders and Bi Nanoparticles as Cocatalyst, Adv.Mater. Interfaces, 2 (2015) 1500249.

[161] H. Wang, W. Zhang, X. Li, J. Li, W. Cen, Q. Li, F. Dong, Highly enhanced visible light photocatalysis and in situ FT-IR studies on Bi metal @defective BiOCl hierarchical microspheres, Appl. Catal. B: Environ., 225 (2018) 218-227.

[162] J. Feng, X. Qian, C.-W. Huang, J. Li, Strain-engineered artificial atom as a broad-spectrum solar energy funnel, Nature Photonics 6 (2012) 866-872.

[163] H. Feng, J. Zhuang, A.D. Slattery, L. Wang, Z. Xu, X. Xu, D. Mitchell, T. Zheng, S. Li, M. Higgins, L. Ren, Z. Sun, S.X. Dou, Y. Du, W. Hao, Construction of 2D lateral pseudoheterostructures

by strain engineering, 2D Mater., 4 (2017) 025102

[164] H. Feng, Z. Xu, L. Wang, Y. Yu, D. Mitchell, D. Cui, X. Xu, J. Shi, T. Sannomiya, Y. Du, W. Hao, S.X. Dou, Modulation of photocatalytic properties by strain in 2D BiOBr Nanosheets, ACS Appl. Mater. Inter., 7 (2015) 27592-27596.

[165] X. Jia, J. Cao, H. Lin, Y. Chen, W. Fu, S. Chen, One-pot synthesis of novel flower-like $BiOBr_{0.9}I_{0.1}/BiOI$ heterojunction with largely enhanced electron-hole separation efficiency and photocatalytic performances, J. Mol. Catal. A-Chem., 409 (2015) 94-101.

[166] T. Wu, X. Li, D. Zhang, F. Dong, S. Chen, Efficient visible light photocatalytic oxidation of NO with hierarchical nanostructured 3D flower-like $BiOCl_xBr_{1-x}$ solid solutions, J. Alloys Compd., 671 (2016) 318-327.

[167] X. Zhang, L.W. Wang, C.Y. Wang, W.K. Wang, Y.L. Chen, Y.X. Huang, W.W. Li, Y.J. Feng, H.Q. Yu, Synthesis of $BiOCl_xBr_{1-x}$ nanoplate solid solutions as a robust photocatalyst with tunable band structure, Chemistry 21 (2015) 11872-11877.

[168] W.J. Kim, D. Pradhan, B.-K. Min, Y. Sohn, Adsorption/photocatalytic activity and fundamental natures of BiOCl and $BiOCl_xI_{1-x}$ prepared in water and ethylene glycol environments, and Ag and Au-doping effects, Appl. Catal. B: Environ., 147 (2014) 711-725.

[169] C.-Y. Wang, X. Zhang, Y.-J. Zhang, J.-J. Chen, G.-X. Huang, J. Jiang, W.-K. Wang, H.-Q. Yu, Direct generation of hydroxyl radicals over bismuth oxybromide nanobelts with tuned band structure for photocatalytic pollutant degradation under visible light irradiation, Appl. Catal. B: Environ., 237 (2018) 464-472.

[170] L. Wang, J. Shang, W. Hao, S. Jiang, S. Huang, T. Wang, Z. Sun, Y. Du, S. Dou, T. Xie, D. Wang, J. Wang, A dye-sensitized visible light photocatalyst-$Bi_{24}O_{31}Cl_{10}$, Sci. Rep., 4 (2014) 7384.

[171] X. Mao, F. Xie, M. Li, Facile hydrolysis synthesis of novel $Bi_4O_5Br_2$ photocatalyst with enhanced visible light photocatalytic activity for the degradation of resorcinol, Mater. Lett., 166 (2016) 296-299.

[172] Y. Su, C. Ding, Y. Dang, H. Wang, L. Ye, X. Jin, H. Xie, C. Liu, First hydrothermal synthesis of $Bi_5O_7Br$ and its photocatalytic properties for molecular oxygen activation and RhB degradation, Appl. Surf. Sci., 346 (2015) 311-316.

[173] B. Sarwan, B. Pare, A.D. Acharya, The effect of oxygen vacancies on the photocatalytic activity of BiOCl nanocrystals prepared by hydrolysis and UV light irradiation, Mat. Sci. Semicon. Proc., 25 (2014) 89-97.

[174] X.J. Wang, Y. Zhao, F.T. Li, L.J. Dou, Y.P. Li, J. Zhao, Y.J. Hao, A chelation strategy for in-situ constructing surface oxygen vacancy on {001} facets exposed BiOBr nanosheets, Sci. Rep., 6 (2016) 24918.

[175] M. He, W. Li, J. Xia, X. Li, J. Di, H. Xu, S. Yin, H. Li, M. Li, The enhanced visible light photocatalytic activity of yttrium-doped BiOBr synthesized via a reactable ionic liquid, Appl. Surf. Sci., 331 (2015) 170-178.

[176] A. Dash, S. Sarkar, V.N. Adusumalli, V. Mahalingam, Microwave synthesis, photoluminescence, and photocatalytic activity of PVA-functionalized $Eu^{3+}$-doped BiOX (X = Cl, Br, I) nanoflakes, Langmuir 30 (2014) 1401-1409.

[177] K. Xu, X. Fu, Z. Peng, Facile synthesis and photocatalytic activity of La-doped BiOCl hierarchical, flower-like nano-/micro-structures, Mater. Res. Bull., 98 (2017) 103-110.

[178] H. Yi, L. Qin, D. Huang, G. Zeng, C. Lai, X. Liu, B. Li, H. Wang, C. Zhou, F. Huang, S. Liu, X. Guo, Nano-structured bismuth tungstate with controlled morphology: Fabrication, modification, environmental application and mechanism insight, Chem. Eng. J., 358 (2019) 480-496.

[179] C. Zhang, W. Wang, A. Duan, G. Zeng, D. Huang, C. Lai, X. Tan, M. Cheng, R. Wang, C. Zhou, W. Xiong, Y. Yang, Adsorption behavior of engineered carbons and carbon nanomaterials for metal endocrine disruptors: Experiments and theoretical calculation, Chemosphere 222 (2019) 184-194.

[180] C. Ming, G. Zeng, L. Cui, Z. Chang, P. Xu, Y. Min, W. Xiong, Interactions of carbon nanotubes and/or graphene with manganese peroxidase during biodegradation of endocrine disruptors and triclosan, Chemosphere 184 (2017) 127-136.

[181] M. Chen, X. Qin, G. Zeng, Single-walled carbon nanotube release affects the microbial enzyme-catalyzed oxidation processes of organic pollutants and lignin model compounds in nature, Chemosphere 163 (2016) 217-226.

[182] W. Xue, D. Huang, G. Zeng, J. Wan, C. Zhang, R. Xu, M. Cheng, R. Deng, Nanoscale zero-valent iron coated with rhamnolipid as an effective stabilizer for immobilization of Cd and Pb in river sediments, J. Hazar. Mater., 341 (2017) 381.

[183] F. Perreault, A. Fonseca de Faria, M. Elimelech, Environmental applications of graphene-based nanomaterials, Chem. Soc. Rev., 44 (2015) 5861-5896.

[184] C. Zhou, P. Xu, C. Lai, C. Zhang, G. Zeng, D. Huang, M. Cheng, L. Hu, W. Xiong, X. Wen, L. Qin, J. Yuan, W. Wang, Rational design of graphic carbon nitride copolymers by molecular doping for visible-light-driven degradation of aqueous sulfamethazine and hydrogen evolution, Chem. Eng. J., 359 (2019) 186-196.

[185] D. Jiang, P. Xu, H. Wang, G. Zeng, D. Huang, M. Chen, C. Lai, C. Zhang, J. Wan, W. Xue, Strategies to improve metal organic frameworks photocatalyst's performance for degradation of organic pollutants, Coordin. Chem. Rev., 376 (2018) 449-466.

[186] M. Cheng, C. Lai, Y. Liu, G. Zeng, D. Huang, C. Zhang, L. Qin, L. Hu, C. Zhou, W. Xiong,

Metal-organic frameworks for highly efficient heterogeneous Fenton-like catalysis, Coordin. Chem. Rev., (2018) 80–92.

[187] A. Sivakumar, B. Murugesan, A. Loganathan, P. Sivakumar, A review on decolourisation of dyes by photodegradation using various bismuth catalysts, J. Taiwan Inst Chem. E., 45 (2014) 2300-2306.

[188] M.T. Yagub, T.K. Sen, S. Afroze, H.M. Ang, Dye and its removal from aqueous solution by adsorption: a review, Adv. Colloid. Interfac., 209 (2014) 172-184.

[189] A. Ajmal, I. Majeed, R.N. Malik, H. Idriss, M.A. Nadeem, Principles and mechanisms of photocatalytic dye degradation on $TiO_2$ based photocatalysts: a comparative overview, RSC Adv., 4 (2014) 37003-37026.

[190] D. Chu, X. Dong, Q. Zhao, J. Gu, Z. Wang, Photosensitization priming of tumor microenvironments improves delivery of nanotherapeutics via neutrophil infiltration, Adv. Mater., 29 (2017) 1701021.

[191] K. Ren, J. Liu, J. Liang, K. Zhang, X. Zheng, H. Luo, Y. Huang, P. Liu, X. Yu, Synthesis of the bismuth oxyhalide solid solutions with tunable band gap and photocatalytic activities, Dalton. Trans., 42 (2013) 9706-9712.

[192] Y.L. Qi, Y.F. Zheng, X.C. Song, Synthesis and enhanced visible light photocatalytic activity of $WO_3$-$BiOCl_xBr_{1-x}$ heterojunctions with tunable energy band structure, Ceram. Int., 43 (2017) 12302-12310.

[193] M. Cheng, G. Zeng, D. Huang, C. Lai, Y. Liu, C. Zhang, J. Wan, L. Hu, C. Zhou, W. Xiong, Efficient degradation of sulfamethazine in simulated and real wastewater at slightly basic pH values using Co-SAM-SCS /$H_2O_2$ Fenton-like system, Water Res., 138 (2018) 7-18.

[194] L. Qin, D. Huang, P. Xu, G. Zeng, C. Lai, Y. Fu, H. Yi, B. Li, C. Zhang, M. Cheng, C. Zhou, X.

Wen, In-situ deposition of gold nanoparticles onto polydopamine-decorated g-$C_3N_4$ for highly efficient reduction of nitroaromatics in environmental water purification, J. Colloid Interface Sci., 534 (2019) 357-369.

[195] Y. Bai, P. Yang, P. Wang, Z. Fan, H. Xie, P.K. Wong, L. Ye, Solid phase fabrication of Bismuth-rich $Bi_3O_4Cl_xBr_{1-x}$ solid solution for enhanced photocatalytic NO removal under visible light, J. Taiwan Inst Chem. E., 82 (2018) 273-280.

[196] C.-C. Wang, J.-R. Li, X.-L. Lv, Y.-Q. Zhang, G. Guo, Photocatalytic organic pollutants degradation in metal–organic frameworks, Energ. Environ. Sci., 7 (2014) 2831-2867.

[197] R. Li, J. Liu, X. Zhang, Y. Wang, Y. Wang, C. Zhang, X. Zhang, C. Fan, Iodide-modified $Bi_4O_5Br_2$ photocatalyst with tunable conduction band position for efficient visible-light decontamination of pollutants, Chem. Eng. J., 339 (2018) 42-50.

[198] Y. Boyjoo, H. Sun, J. Liu, V.K. Pareek, S. Wang, A review on photocatalysis for air treatment: From catalyst development to reactor design, Chem. Eng. J., 310 (2017) 537-559.

[199] X. Wu, K. Zhang, G. Zhang, S. Yin, Facile preparation of BiOX (X=Cl, Br, I) nanoparticles and up-conversion phosphors/BiOBr composites for efficient degradation of NO gas: Oxygen vacancy effect and near infrared light responsive mechanism, Chem. Eng. J., 325 (2017) 59-70.

[200] Z. Zhao, Y. Cao, F. Dong, F. Wu, B. Li, Q. Zhang, Y. Zhou, The activation of oxygen through oxygen vacancies in BiOCl/PPy to inhibit toxic intermediates and enhance the activity of photocatalytic nitric oxide removal, Nanoscale 11 (2019) 6360-6367.

[201] D. Xia, L. Hu, C. He, W. Pan, T. Yang, Y. Yang, D. Shu, Simultaneous photocatalytic elimination of gaseous NO and $SO_2$ in a $BiOI/Al_2O_3$-padded trickling scrubber under visible light, Chem. Eng. J., 279 (2015) 929-938.

[202] G. Liu, T. Wang, S. Ouyang, L. Liu, H. Jiang, Q. Yu, T. Kako, J. Ye, Band-structure-controlled BiO(ClBr)$_{(1-x)/2}$I$_x$ solid solutions for visible-light photocatalysis, J. Mater. Chem., A 3 (2015) 8123-8132.

[203] X. Wei, X. Wang, Q. An, C. Han, L. Mai, Operando x-ray diffraction characterization for understanding the intrinsic electrochemical mechanism in rechargeable battery materials, Small Methods 1 (2017) 1700083.

[204] J. Wu, H. Shan, W. Chen, X. Gu, P. Tao, C. Song, W. Shang, T. Deng, In situ environmental TEM in imaging gas and liquid phase chemical reactions for materials research, Adv. Mater., 28 (2016) 9686-9712.